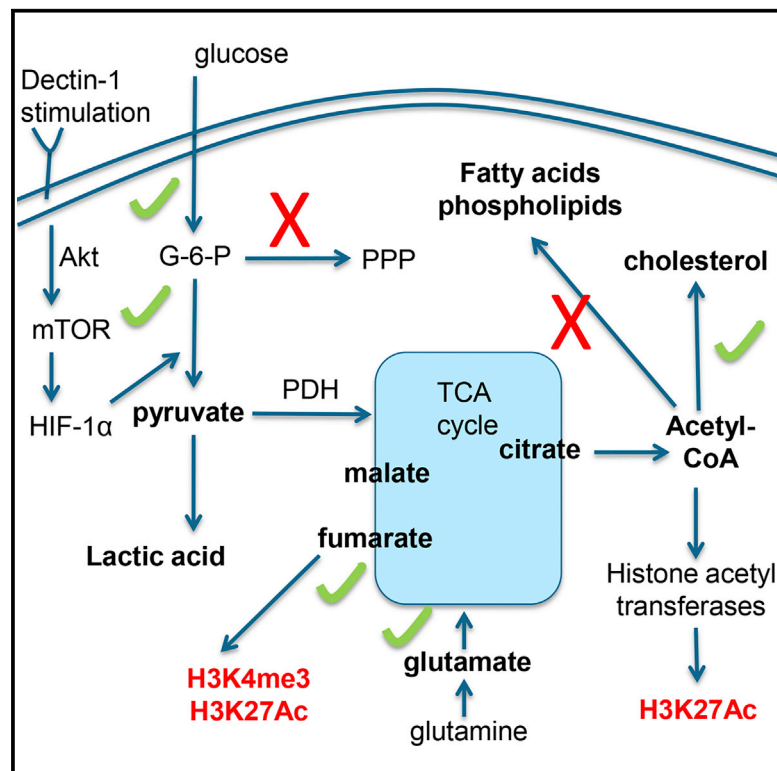# Glutaminolysis and Fumarate Accumulation Integrate Immunometabolic and Epigenetic Programs in Trained Immunity

Graphical Abstract

Authors

Rob J.W. Arts, Boris Novakovic, Rob ter Horst, ..., Hendrik G. Stunnenberg, Ramnik J. Xavier, Mihai G. Netea

Correspondence

rob.jw.arts@radboudumc.nl

In Brief

As part of the IHEC consortium, Arts et al. dissect how metabolic pathways regulate epigenetic rewiring in trained immunity (innate immune memory). They show that glycolysis, glutaminolysis, and cholesterol metabolism are indispensable in trained monocytes and link fumarate accumulation to epigenetic changes. Explore the Cell Press IHEC webportal at http://www.cell.com/consortium/IHEC.

Highlights

- Cellular metabolism undergoes major shifts in β-glucan-trained monocytes

- Glucose, glutamine, and cholesterol metabolism are crucial in trained immunity

- Accumulation of fumarate is essential for epigenetic changes in trained immunity

Accession Numbers

GSE85246
GSE86940

Article

Glutaminolysis and Fumarate Accumulation Integrate Immunometabolic and Epigenetic Programs in Trained Immunity

Rob J.W. Arts,[1,12,*] Boris Novakovic,[2] Rob ter Horst,[1] Agostinho Carvalho,[3,4] Siroon Bekkering,[1] Ekta Lachmandas,[1] Fernando Rodrigues,[3,4] Ricardo Silvestre,[3,4] Shih-Chin Cheng,[1,5] Shuang-Yin Wang,[2] Ehsan Habibi,[2] Luís G. Gonçalves,[6] Inês Mesquita,[3,4] Cristina Cunha,[3,4] Arjan van Laarhoven,[1] Frank L. van de Veerdonk,[1] David L. Williams,[7] Jos W.M. van der Meer,[1] Colin Logie,[2] Luke A. O'Neill,[8] Charles A. Dinarello,[1,9] Niels P. Riksen,[1] Reinout van Crevel,[1] Clary Clish,[10] Richard A. Notebaart,[1] Leo A.B. Joosten,[1] Hendrik G. Stunnenberg,[2] Ramnik J. Xavier,[10,11] and Mihai G. Netea[1]

[1]Department of Internal Medicine, Radboud University Medical Center, 6525 GA Nijmegen, the Netherlands
[2]Department of Molecular Biology, Faculty of Science, Radboud University, 6525 HP Nijmegen, the Netherlands
[3]Life and Health Sciences Research Institute (ICVS), School of Health Sciences, University of Minho, 4710-057 Braga, Portugal
[4]ICVS/3B's - PT Government Associate Laboratory, 4806-909 Braga/Guimarães, Portugal
[5]Institute of Molecular Medicine, National Tsing Hua University, 300 Hsinchu City, Taiwan
[6]Instituto de Tecnologia Química e Biológica António Xavier, Universidade Nova de Lisboa, 2780-157 Oeiras, Portugal
[7]Department of Surgery, Quillen College of Medicine and Center for Inflammation, Infectious Disease and Immunity, East Tennessee State University, Johnson City, TN 37604, USA
[8]Trinity Biomedical Sciences Institute, Trinity College, Dublin 2, Ireland
[9]Department of Medicine, University of Colorado Denver, Aurora, CO 80045, USA
[10]Broad Institute of Harvard University and Massachusetts Institute of Technology, Cambridge, MA 02142, USA
[11]Center for Computational and Integrative Biology and Gastrointestinal Unit and Center for the Study of Inflammatory Bowel Disease, Massachusetts General Hospital, Boston, MA 02114, USA
[12]Lead Contact
*Correspondence: rob.jw.arts@radboudumc.nl
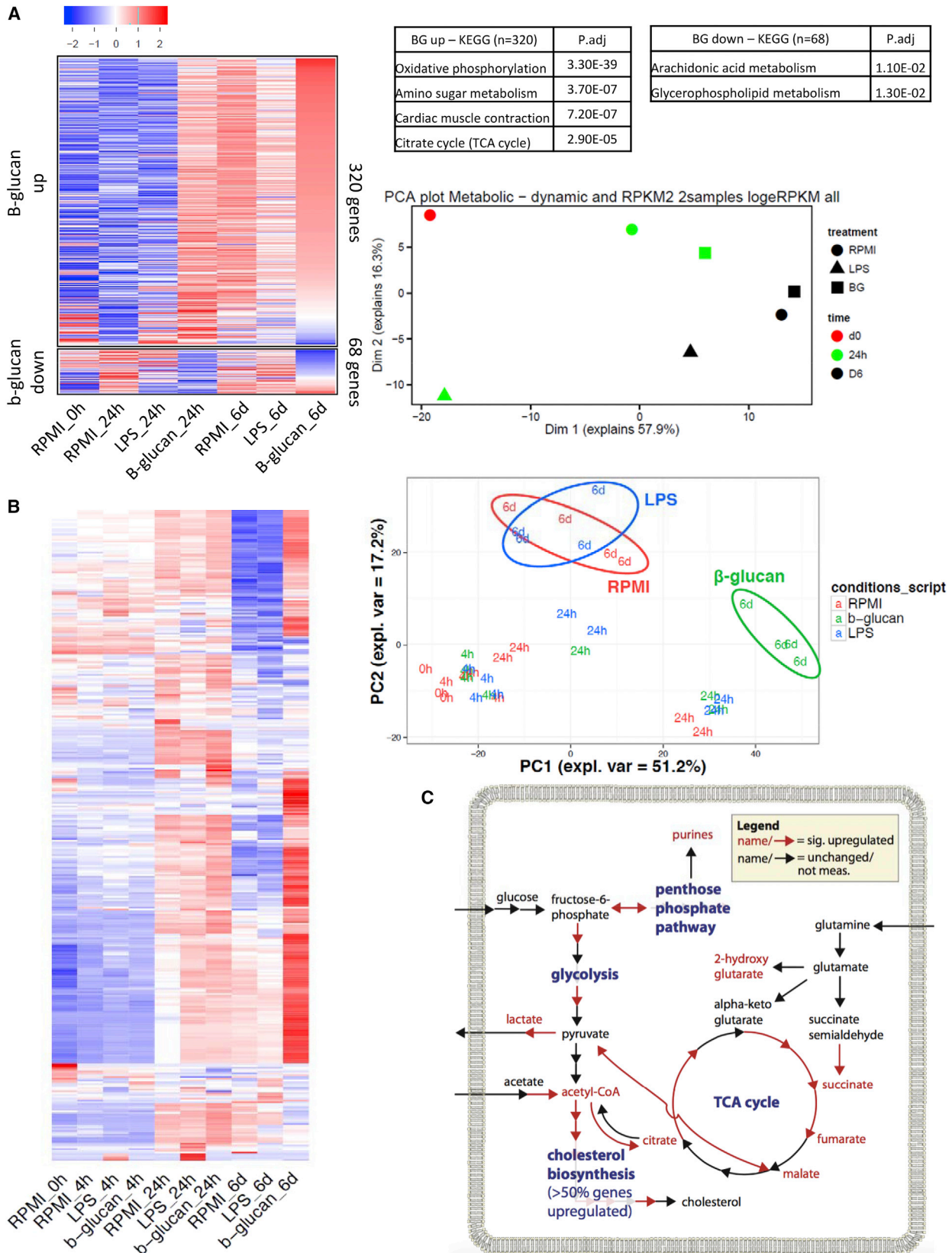http://dx.doi.org/10.1016/j.cmet.2016.10.008

SUMMARY

Induction of trained immunity (innate immune memory) is mediated by activation of immune and metabolic pathways that result in epigenetic rewiring of cellular functional programs. Through network-level integration of transcriptomics and metabolomics data, we identify glycolysis, glutaminolysis, and the cholesterol synthesis pathway as indispensable for the induction of trained immunity by β-glucan in monocytes. Accumulation of fumarate, due to glutamine replenishment of the TCA cycle, integrates immune and metabolic circuits to induce monocyte epigenetic reprogramming by inhibiting KDM5 histone demethylases. Furthermore, fumarate itself induced an epigenetic program similar to β-glucan-induced trained immunity. In line with this, inhibition of glutaminolysis and cholesterol synthesis in mice reduced the induction of trained immunity by β-glucan. Identification of the metabolic pathways leading to induction of trained immunity contributes to our understanding of innate immune memory and opens new therapeutic avenues.

INTRODUCTION

Recent studies demonstrated that certain infections and vaccinations induce innate immune memory (also termed trained immunity; Netea et al., 2016) in monocytes, macrophages, and natural killer cells, resulting in non-specific protection against reinfection (Quintin et al., 2012; Sun et al., 2009). The biological relevance of innate immune memory is demonstrated by its broad presence in nature, with studies in organisms as diverse as plants, insects, cephalopods, and mammals reporting its impact for resistance to infections (Fu and Dong, 2013; Kurtz, 2005; Netea et al., 2011). Many of the studies reporting adaptive characteristics embedded in innate immune responses predate the modern era of molecular biology: the lack of understanding the molecular mechanisms underlying their effects impaired, however, the capacity to fully understand the importance of this process. This situation has changed profoundly over the last few years, when several studies demonstrated that epigenetic reprogramming forms the basis of innate immune memory in both plants (Muthamilarasan and Prasad, 2013; Shah et al., 2014) and mammals (Kleinnijenhuis et al., 2012; O'Sullivan et al., 2015; Quintin et al., 2012; Saeed et al., 2014).

Genome-wide changes in histone modifications have been shown to underlie trained immunity in monocytes, but the molecular mechanisms linking the immunological signals induced by microbial stimuli or vaccines to the epigenetic changes have not been deciphered. Changes in cellular metabolism, with a shift from oxidative phosphorylation to aerobic glycolysis (Warburg effect), are crucial for the induction of β-glucan-induced trained immunity (Cheng et al., 2014). Interestingly, increasing evidence links cellular metabolism to the regulation of gene transcription, as several metabolites from glycolysis and the TCA cycle have been shown to act as cofactors for epigenetic writers and erasers such as DNA and histone methyltransferases and

A

BG up – KEGG (n=320)	P.adj
Oxidative phosphorylation	3.30E-39
Amino sugar metabolism	3.70E-07
Cardiac muscle contraction	7.20E-07
Citrate cycle (TCA cycle)	2.90E-05

BG down – KEGG (n=68)	P.adj
Arachidonic acid metabolism	1.10E-02
Glycerophospholipid metabolism	1.30E-02

B

C

demethylases and histone acetyltransferases and deacetylases (Donohoe and Bultman, 2012; Hirschey et al., 2015). These circuits have important functional consequences based on how cells use metabolic substrates: for example, type 1 inflammatory macrophages (M[IFNγ]) rely on increased glycolysis (Mills and O'Neill, 2015; Pearce et al., 2013; Tan et al., 2015), whereas tolerant macrophages (M[IL-4]) rely on oxidative phosphorylation and β-oxidation (Mills and O'Neill, 2015; Van den Bossche et al., 2015). Interestingly, not only glucose metabolism, but also other metabolic pathways play important roles in reprogramming and polarizing cells (Cheng et al., 2016; Donohoe and Bultman, 2012; Hirschey et al., 2015).

Based on this growing body of evidence, we hypothesized that changes in cellular metabolism in trained immunity not only reflect enhanced energetic needs, but also connect with immune pathways and epigenetic reprogramming, through the accumulation of specific metabolites modulating epigenetic processes that impact the functional program of the cell. We combined transcriptomic, metabolomic, and epigenomic studies to identify important metabolic processes activated in β-glucan-trained monocytes. We validated the role of these processes in induction of trained immunity, identifying an important function for glutamine metabolism and fumarate accumulation. The importance of these processes was also demonstrated in in vivo models of trained immunity.

RESULTS

Cellular Metabolic Pathways in Monocytes during Induction of Trained Immunity

β-glucan and bacterial lipopolysaccharide (LPS) induce different long-term functional programs in monocytes and macrophages; i.e., enhanced function and tolerance, respectively; with transcriptomic and epigenomic analyses revealing major differences in glucose metabolism pathways (Cheng et al., 2014; Saeed et al., 2014). To elucidate whether additional metabolic pathways are differentially expressed between trained and tolerant cells, RNA-sequencing (seq) expression data at different time points after stimulation with β-glucan and LPS were analyzed for metabolic pathways and full intracellular metabolome assessment was performed. We used the previously described in vitro model of trained immunity (Cheng et al., 2014) in which purified monocytes are stimulated for 24 hr with RPMI, β-glucan, or LPS, after which cells are washed and rested for 5 days in culture medium, followed by a second 24 hr stimulation with either medium or LPS (Figure S1). Distinct RNA expression patterns between β-glucan-trained and non-trained (RPMI) cells were

visible after 24 hr of stimulation, with the largest differences observed at the day 6 time point in LPS-treated cells (Figure 1A; Table S1). Metabolome data of trained and tolerant cells showed that at early time points (4 hr and 24 hr after stimulation), only small differences existed between the three conditions (RPMI, LPS, β-glucan). On day 6, however, the intracellular metabolome of β-glucan-trained cells was clearly different from the RPMI and LPS-treated cells, with major differences observed in TCA cycle metabolites, fatty acid metabolism, and other pathways (Figures 1B and S1; Tables S2 and S3). Altogether, these data indicate that the majority of transcriptional changes associated with metabolic pathways occur early (24 hr) in β-glucan-exposed cells and precede the metabolic phenotype observed in fully differentiated β-glucan-trained macrophages on day 6.

Integration of the transcriptome and metabolome data in a network-level context revealed an upregulation of several major metabolic pathways in β-glucan-trained macrophages, including glycolysis, pentose phosphate pathway (PPP), and cholesterol metabolism (Figures 1C and S1). Interestingly, several important TCA metabolites were strongly increased, such as succinate, malate, and fumarate, as well as 2-hydroxyglutarate, leading us to hypothesize that TCA metabolites were being replenished through glutaminolysis (Figures 1C and S1).

Glycolysis, but Not PPP, Is an Essential Metabolic Pathway in Trained Immunity

Glucose consumption is increased in β-glucan-trained macrophages (Cheng et al., 2014), and our metabolome analysis supports an increase in glycolysis. To obtain further insight into the major accumulated products of glucose metabolism, we performed NMR experiments with ^{13}C-labeled glucose in trained monocytes. First, glucose was converted into lactate, validating the upregulation of glycolysis with concomitant lactate production in β-glucan-trained monocytes that we reported previously (Cheng et al., 2014). In addition, labeled purines were also detected, showing the activation of the PPP (Figures 2A and S2). In contrast, neither ^{13}C-labeled metabolites of the TCA cycle were detected after incubation of trained monocytes with ^{13}C-labeled glucose, nor 3-^{13}C lactate, indicating that the non-oxidative branch from the PPP back to glycolysis was inactive (Figures 2A and S2).

As glucose can be metabolized by aerobic glycolysis and PPP, we assessed which of these pathways was important for induction of trained immunity. Inhibition of mTOR and glycolytic flux by rapamycin inhibited monocyte training, as previously shown (Cheng et al., 2014), whereas inhibition of the oxidative

Figure 1. Metabolism in Trained and Tolerant Macrophages
(A) Heatmap depicting average mRNA expression of β-glucan-modulated metabolism-associated genes. The rows indicate different gene transcripts, and the columns indicate different conditions and time points. Log(e)RPKM values were Z scored and then plotted, with red indicating high RNA expression and blue indicating low RNA expression. The PCA plot shows the relationship between samples based on the expression of dynamic metabolic genes. RPMI (circles), LPS (triangles), and β-glucan (squares) samples are shown at 24 hr (green) and day 6 (black). See also Table S1.
(B) Heatmap depicting the average metabolite intensities in the metabolomics data. The rows indicate different metabolites, and the columns indicate different conditions. The log transformed metabolite intensities were first Z scored/standardized and then averaged over all replicates. A PCA score plot of PC1 versus PC2 of the standardized metabolomics data is shown. The samples are color-coded according to the stimulus that was used, and the labels indicate time points after stimulation. See also Figure S1 and Tables S2 and S3.
(C) Schematic pathway map depicting gene expression (arrows) and metabolic changes (filled circles) in cells treated with β-glucan versus LPS at day 6. The transcripts and metabolites marked in red were significantly upregulated in β-glucan versus LPS. The complete map as created by Escher is depicted in Figure S1.

CellPress
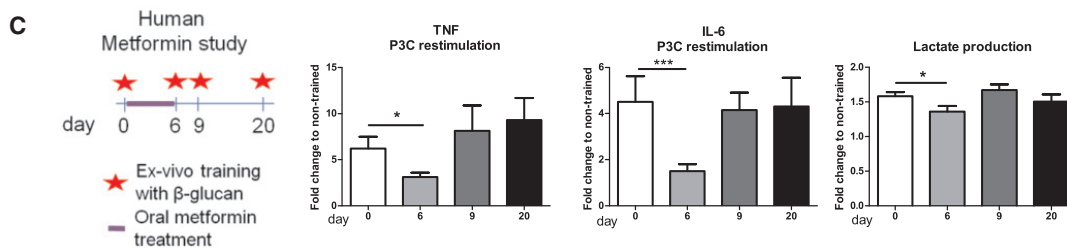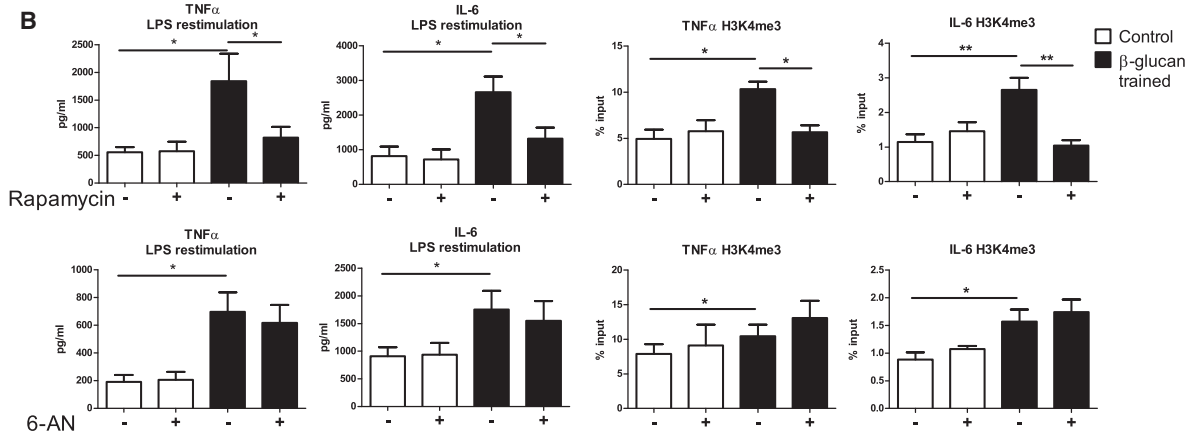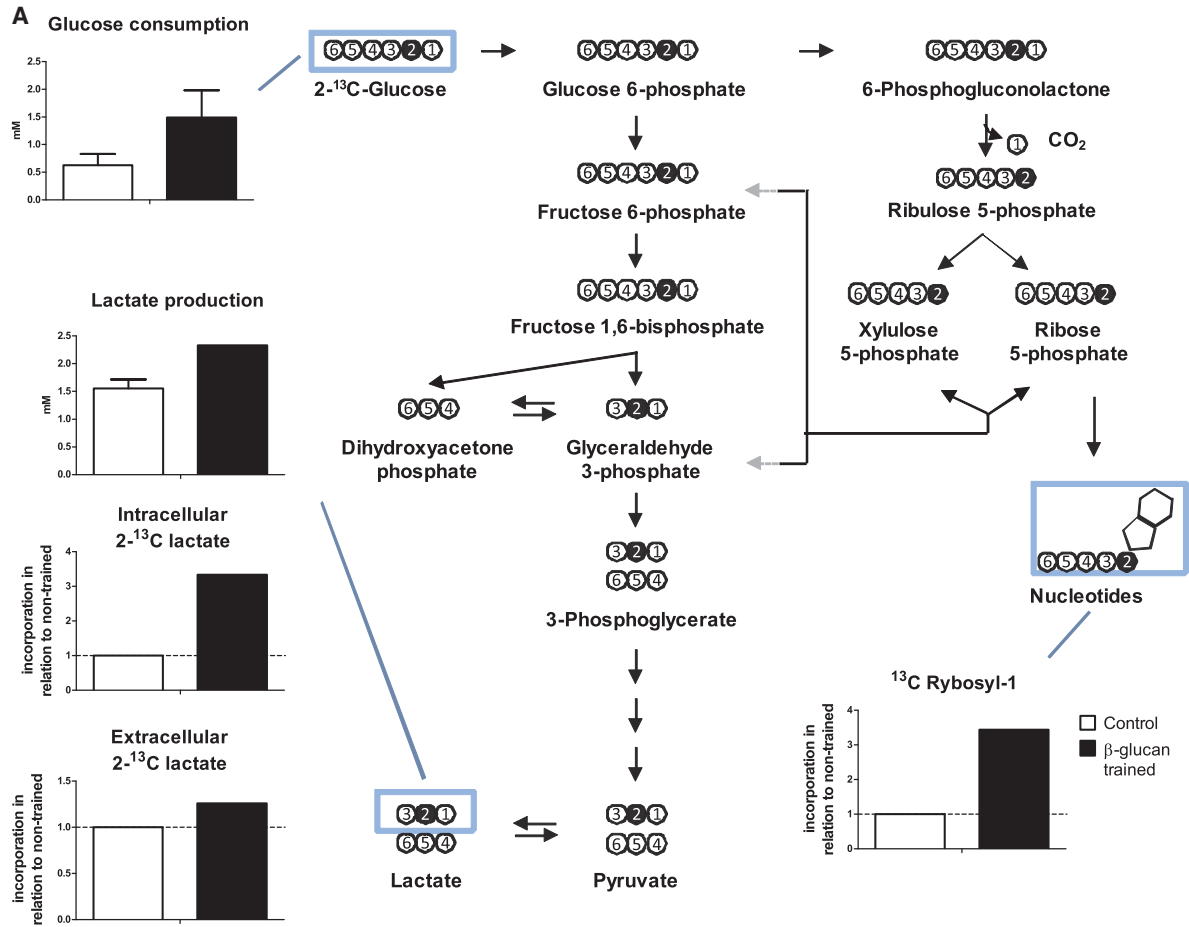
(legend on next page)

branch of the PPP by 6-aminonicotinamide (6-AN) had no effect (Figure 2B). The increase in cytokine production by β-glucan-induced trained immunity is accompanied by epigenetic changes, including an increase of H3K4 trimethylation (H3K4me3) at promoter sites of inflammatory genes (Saeed et al., 2014). Consistent with similar observations in cytokine production, epigenetic changes in H3K4me3 induced by β-glucan at the promoter sites of *IL6* and *TNFA* were abolished by rapamycin, but not by 6-AN (Figures 2B and S3). Thus, whereas glycolysis is central for induction of trained immunity, inhibition of PPP does not have a direct effect on increased cytokine production by trained monocytes.

Metformin activates AMPK and inhibits mTOR activity (Figure S3) (Cheng et al., 2016). We have previously shown that inhibition of the mTOR pathway that controls glucose metabolism by metformin counteracts the induction of trained immunity by β-glucan in mice (Cheng et al., 2014). We now also show that metformin inhibits lactate production, 5 days after β-glucan training (Figure S3). To assess whether metformin has a similar effect in vivo in humans, we initiated a proof-of-principle clinical trial in which healthy volunteers received an incremental dose of metformin for 6 days (up to 1,000 mg twice daily on day 6). In line with the in vitro and murine experimental data, in vivo administration of metformin in humans decreased the ex-vivo β-glucan-induced training of circulating monocytes, which was accompanied by a lower capacity to mount glycolysis and release lactate (Figure 2C). When the study participants stopped taking metformin, the capacity of monocytes to undergo β-glucan training was fully restored (day 9 and 20), thereby confirming the importance of glucose metabolism changes for inducing trained immunity in humans (Figure 2C).

Glutamine and Cholesterol Metabolism Are Important Metabolic Pathways in Trained Immunity

In addition to glycolysis and PPP, glutamine metabolism, cholesterol, and fatty acid synthesis pathways were also upregulated after β-glucan training. Glutamine metabolism has been shown to play an important role in immune activation (Li et al., 2007; Roth, 2008; Sikalidis, 2015). Incubation of trained monocytes with ^{13}C-labeled glutamine resulted in increased production of glutamate, a substrate that can replenish the TCA cycle (Figures 3A and S2). Although no labeled succinate, fumarate, or malate were identified due to their relatively low concentrations and the limited sensitivity of the assay, we were able to measure increases in these TCA cycle metabolites using classical biochemical methods (Figures S1 and S4). Interestingly, no labeled lactate was detected, suggesting that glutamine is not a source of pyruvate for lactic fermentation (Figures 3A and

S2). This interpretation was supported by the near 1:2 molar ratio of glucose:lactate observed in the ^{13}C-glucose experiment, suggesting that glucose is the sole source of lactate; the ratio would have been lower if also other sources of lactate would have been used.

Aspartic acid was also consumed in large amounts from the medium, indicating that metabolism of amino acids other than glutamine may also be involved in trained immunity (Figure S4). In line with this notion, production of 2-hydroxyglurate from α-ketoglutarate was also significantly increased, just as methionine (Figure S1). Finally, in addition to the well-known pathway in which glutamate enters the TCA cycle via α-ketoglutarate, glutamate catabolism also enters the TCA cycle via succinate semialdehyde metabolism (Figure 1C).

In an additional set of experiments, we sought to establish the role of glutamine, fatty acid, and cholesterol synthesis in trained immunity by adding inhibitors of these pathways (BPTES, cerulenin, and fluvastatin, respectively) to the in vitro trained immunity model. Inhibition of glutaminolysis or cholesterol synthesis inhibited trained immunity, whereas blockade of fatty acid synthesis had no effect (Figures 3B and S3). In line with these results, H3K4me3 was downregulated by inhibition of either glutaminolysis or cholesterol synthesis (Figure 3B). We next tested the relevance of these pathways in an in vivo model of trained immunity by assessing the effects of BPTES that inhibits glutaminolysis, and atorvastatin, which inhibit the rate-limiting enzyme in cholesterol syntheses HMG-CoA-reductase. Mice were treated with 1 mg of β-glucan or vehicle control intraperitoneally, followed 1 week later by an injection of 10 μg LPS. At 4 hr after the LPS challenge, induction of cytokine synthesis was measured by ELISA in the circulating blood. We found that LPS induced a significantly higher IL-1β concentration in plasma of β-glucan-trained mice than of controls (Figure 3C), as previously reported (Quintin et al., 2012). Importantly, when glutaminolysis was inhibited by BPTES or cholesterol synthesis was inhibited by atorvastatin, trained immunity, measured by IL-1β production, was significantly downregulated (Figure 3C). The plasma concentrations of TNF at this time point after LPS injection were low and not different between the various conditions. Together, these data show that glutaminolysis and the cholesterol synthesis pathway are two metabolic pathways that, in addition to glycolysis, are essential for the increased cytokine production and epigenetic changes observed in β-glucan-induced trained immunity.

## Fumarate Induces Epigenetic Changes and Trained Immunity

Analysis of the metabolome of trained monocytes showed that succinate, fumarate, and malate were strongly induced in these

---

Figure 2. Glucose Metabolism in Trained Immunity

(A) Accumulation of the ^{13}C label that was incorporated in 2-^{13}C labeled glucose was determined in lysates from β-glucan versus non-trained monocytes by NMR, therefore showing to which products glucose is metabolized. The arrows in gray are not active. HSQC-NMR spectra are shown in Figure S2. The data are shown as means ± SEM, n = 2.

(B) Human monocytes were trained with β-glucan or left in culture medium for 24 hr in the presence or absence of mTOR inhibitor (rapamycin) or PPP inhibitor (6-AN). After 6 days, DNA was isolated for epigenetic analysis or cells were restimulated with LPS to determine cytokine production. See also Figure S3. The data are shown as means ± SEM, n = 5, *p < 0.05, **p < 0.01, and Wilcoxon signed-rank test.

(C) Healthy human volunteers received a twice-daily increasing dose (1–2 g) of metformin for 6 days. At indicated time points, monocytes were trained ex vivo with β-glucan; after 5 days of rest, cells were restimulated with P3C and cytokine production was assessed. For the effect of metfomin on the AMPK-mTOR pathway and lactate production, see Figure S3. The data are shown as means ± SEM, n = 11, *p < 0.05, and Wilcoxon signed-rank test.
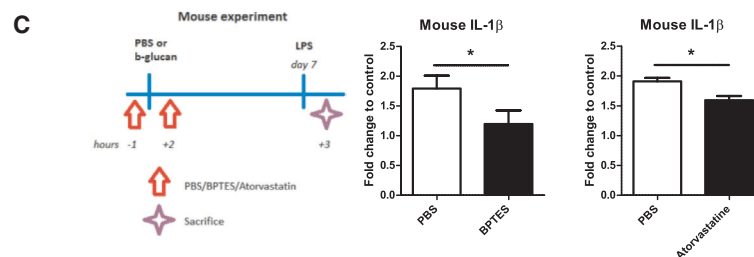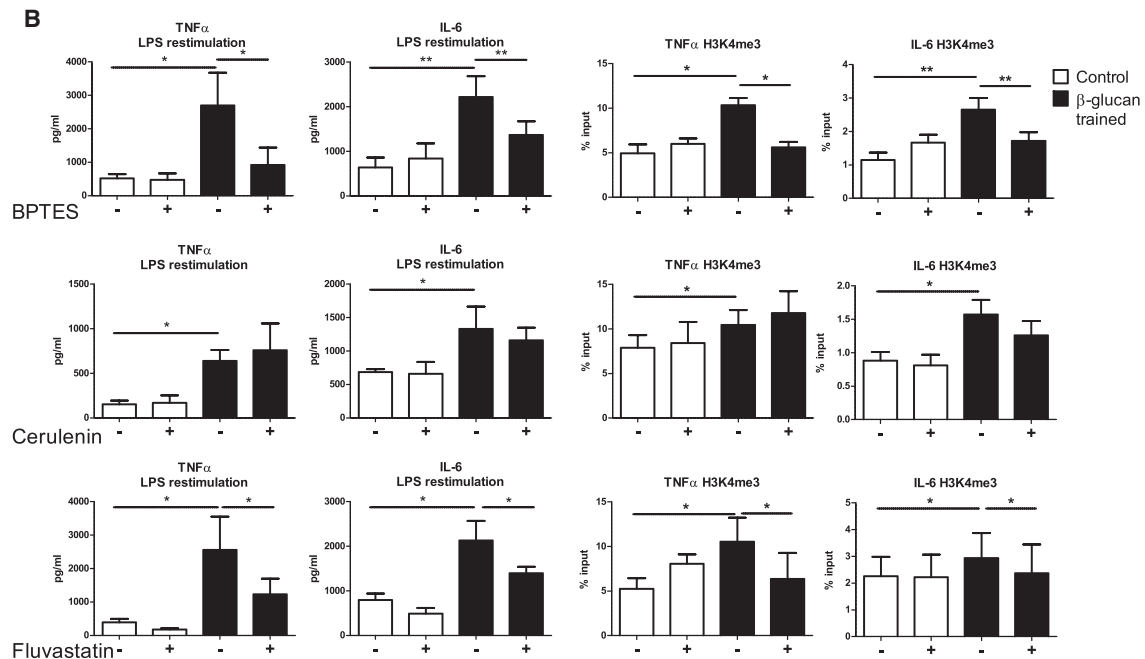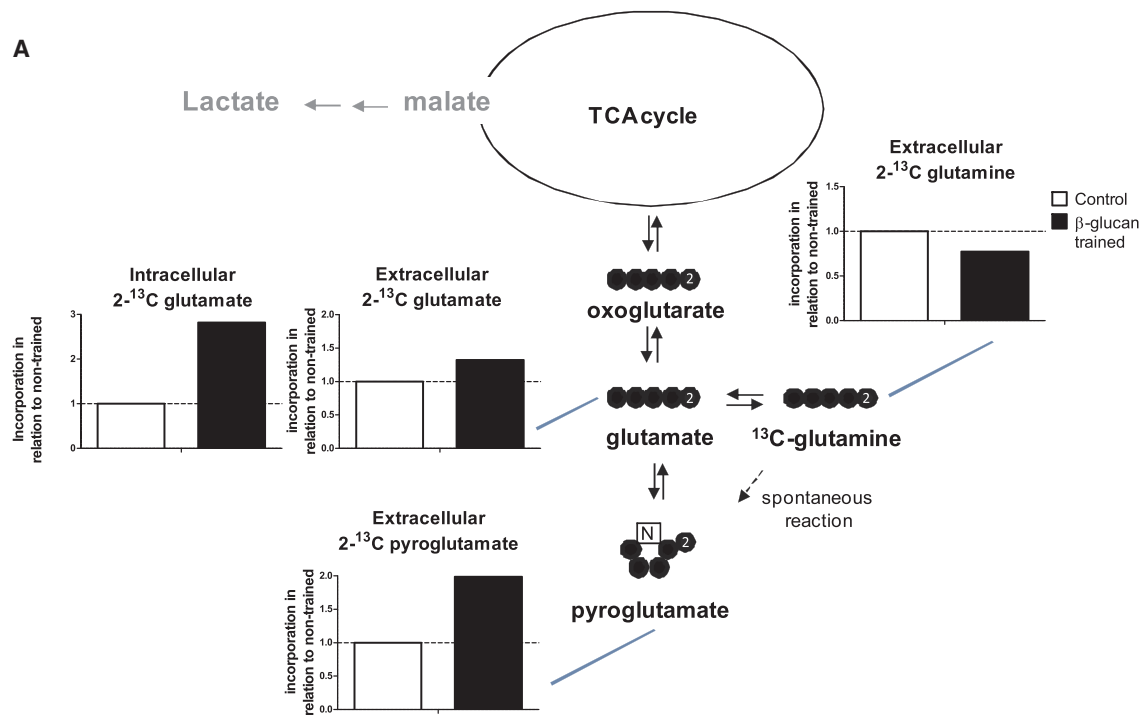
(legend on next page)

cells (Figures 1 and S1). We first assessed whether any of these metabolites by themselves can induce trained immunity. Training of monocytes with fumarate on day 0 dose-dependently induced increased cytokine production upon restimulation on day 6, whereas malate and succinate did not induce this effect (Figure 4A). Inhibition of glycolysis or glutaminolysis by rapamycin or BPTES, respectively, both pathways that inhibit β-glucan-induced trained immunity, also decreased fumarate concentrations in trained monocytes (Figure 4B). In addition, fumarate induced H3K4me3 at the promoters of proinflammatory cytokines, as observed during induction of trained immunity by β-glucan (Figure 4C). Considering these effects, we performed a whole-genome assessment of the histone marks H3K4me3 and H3K27ac by chromatin immunoprecipitation (ChIP)-sequencing in fumarate and β-glucan-trained monocytes (Figure 4D). In total, 124 dynamic H3K4me3 regions (Figure 4E) and 332 dynamic H3K27ac regions (Figure 4F) were identified in fumarate-trained macrophages, with a $\log_2$ fold change >2.5 compared to non-trained macrophages (RPMI). By the same criteria, β-glucan exposure induced 2,688 dynamic H3K27ac changes (Figure S5), indicating that fumarate-induced chromatin remodeling recapitulates only a small fraction of the total trained epigenome. However, 95% of the genomic regions differentially regulated by fumarate were also differentially regulated by β-glucan (>1 $\log_2$ fold change). If for β-glucan a $\log_2$ fold change of >2 were being used, this would account for 63% of the regions. Genes associated with fumarate dynamic epigenetic regions were enriched in pathways involved in immune response and leukocyte migration (Figures 4E and 4F), consistent with previous reports in β-glucan-trained monocytes (Quintin et al., 2012; Saeed et al., 2014).

Citric acid cycle metabolites (e.g., fumarate and succinate) have previously been reported to regulate HIF1α stabilization by inhibiting hydroxylation and therefore stabilizing HIF1α (Koivunen et al., 2007; Tannahill et al., 2013). We first assessed whether fumarate inhibited HIF1α hydroxylation in our in vitro model. Incubation of human monocytes with fumarate for 2 hr inhibited HIF1α hydroxylation (Figure 5A), and HIF1α targets (Ke and Costa, 2006) were induced on a transcriptional level (Figure 5B). This provides a first mechanism of how fumarate could induce the observed phenotypical changes, but it does not explain the observed effects on histone modifications.

Therefore, given our finding that fumarate induces H3K4me3, we investigated whether it could induce transcription of methyltransferases. However, none of the detectable methyltransferases were differentially expressed between trained and non-trained samples (Figure S6). We therefore assessed whether the activity of the KDM5 family of histone demethylases, which are responsible for demethylation of H3K4 (Secombe and Eisenman, 2007), was different in β-glucan trained macrophages. As shown in Figure 5C, β-glucan training of monocytes resulted in decreased biological activity of KDM5 demethylases on day 6 after training, which corresponds to the time point with the highest intracellular fumarate concentrations (Figure S1), an effect that was not observed in LPS-induced immunotolerant macrophages (Figure 5C). Interestingly, a similar effect was observed at transcription level (Figure S6). We also assessed expression of KDM3a/JMJD1a (a H3K9 demethylase) and KDM6b/JMJD3 (a H3K27 demethylase), but these genes were not significantly influenced during induction of training (Figure S6). Finally, as α-ketoglutarate is a known cofactor for lysine demethylases, whereas metabolites that have a comparable molecular structure to α-ketoglutarate (e.g., fumarate or succinate) are natural antagonists (Lu et al., 2012), we also determined whether the effect of fumarate on KDM5 activity is influenced by α-ketogluterate. KDM5 activity was significantly inhibited by fumarate and that was restored by the addition of α-ketoglutarate (Figure 5D). Also at the level of cytokine production, α-ketoglutarate was able to partially counteract the training effect of fumarate (Figure 5E).

DISCUSSION

In this study, we provide the first mechanism linking stimulation of innate immune pathways with the induction of epigenetic and metabolic changes in trained immune cells. We show that training of monocytes with β-glucan induces a rewiring of cellular metabolism that modulates the epigenetic programming of metabolic genes. Glycolysis, glutaminolysis, and cholesterol synthesis are non-redundant metabolic pathways important for trained immunity in monocytes and macrophages. Among the detailed metabolite changes, we identify fumarate as a key metabolite that induces trained immunity (innate immune memory), an effect mediated at least partially by induction of histone modifications such as H3K4me3 and H3K27Ac.

The role of cellular metabolites acting as cofactors for epigenetic enzymes has only recently been revealed in several cell types and tissues (Donohoe and Bultman, 2012; Keating and El-Osta, 2015). By assessing the interaction between transcriptional and metabolic profiles, we identified several major metabolic pathways specifically activated in trained monocytes, compared with naive and tolerant cells. Glucose enters both glycolysis and PPP during activation of trained monocytes. Whereas glycolysis has been previously reported to be important for trained immunity (Cheng et al., 2014), very little is known regarding the role of the PPP in this process. Here, we validate several previous studies of the role of the mTOR pathway and glycolysis and extend them in a proof-of-principle clinical trial.

Figure 3. Other Metabolic Pathways in Trained Immunity

(A) Accumulation of the ^{13}C label that was incorporated in 2-^{13}C labeled glutamine was determined in supernatants and cell lysates from β-glucan versus non-trained monocytes by NMR, therefore showing to which products glutamine is metabolized. HSQC-NMR spectra can be found in Figure S2.

(B) Human monocytes were trained with β-glucan or left in culture medium for 24 hr in the presence or absence of glutaminase inhibitor (BPTES), fatty acid synthesis inhibitor (cerulenin), or HMG-CoA reductase inhibitor (fluvastatin). After 6 days, DNA was isolated for epigenetic analysis or cells were restimulated with LPS to determine cytokine production. See also Figure S3. The data are shown as means ± SEM, n = 5, *p < 0.05, **p < 0.01, and Wilcoxon signed-rank test.

(C) Mice were intraperitoneally trained with β-glucan or PBS in the presence or absence of glutamine (BPTES) or cholesterol (atorvastatin) metabolism inhibitors. After 7 days, an intraperitoneal LPS challenge was performed and IL-1β production was assessed 3 hr later. The fold of increase of IL-1β production of β-glucan trained mice to non-trained mice is shown. The data are shown as means ± SEM, n = 4, *p < 0.05, and paired t test.
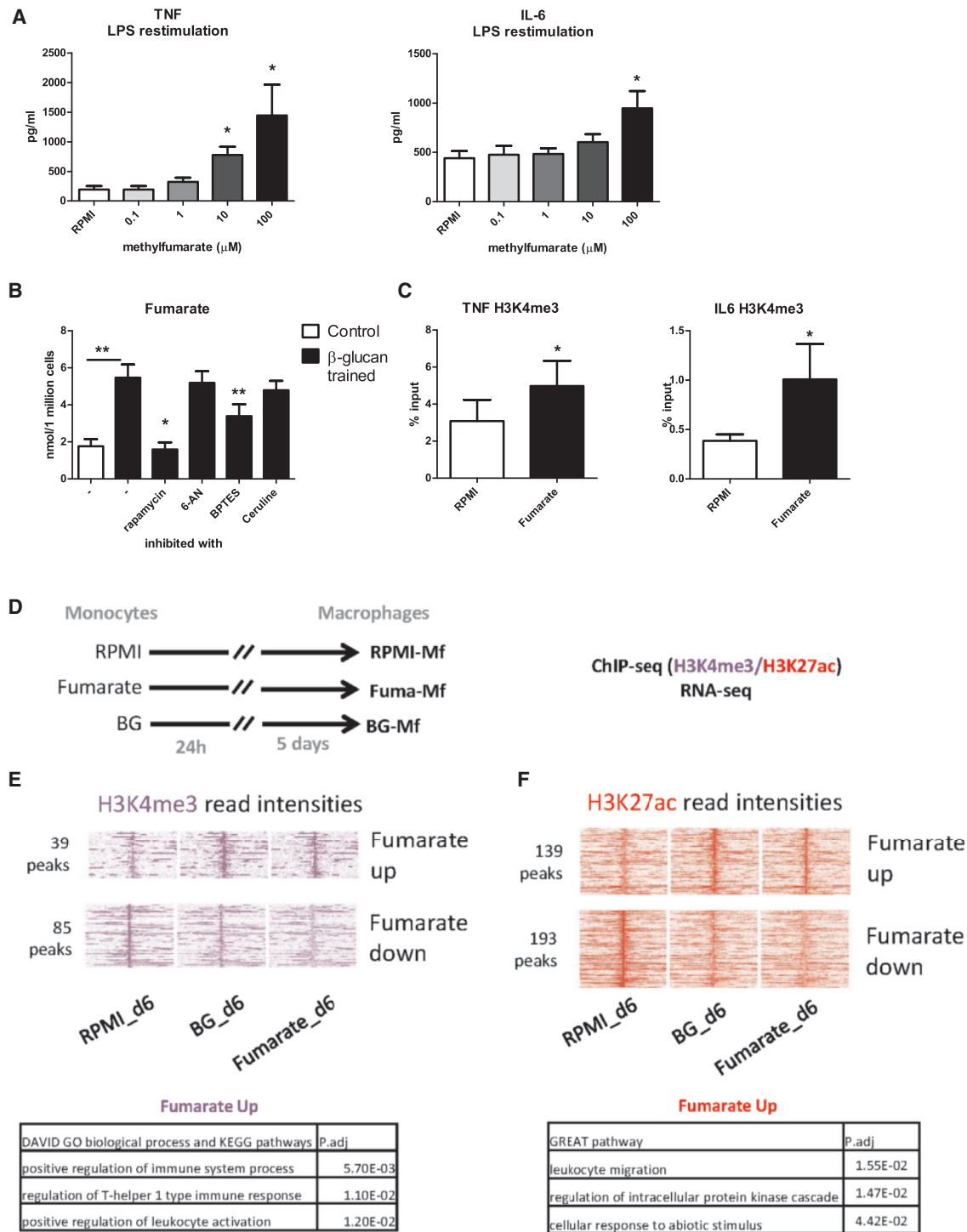
Figure 4. Fumarate-Induced Trained Immunity

(A) Human monocytes were stimulated for 24 hr with different concentrations of methyl-fumarate. At day 6, cells were restimulated for 24 hr with LPS and cytokine production was assessed. The data are shown as means ± SEM, n = 8, *p < 0.05, one-way ANOVA, and Dunnett's post test.

(B) Human monocytes were trained with β-glucan in the presence or absence of metabolic inhibitors for 24 hr. On day 6, cells were lysed and intracellular fumarate concentrations were determined. The data are shown as means ± SEM, n = 9, *p < 0.05, **p < 0.01, and one-way ANOVA.

(C) Human monocytes were stimulated for 24 hr with 50 μM methyl-fumarate. At day 6, cells were fixed, chromatin was isolated, and H3K4me3 at the promoters of *TNFA* and *IL6* were determined. The data are shown as means ± SEM, n = 5, *p < 0.05, and Wilcoxon signed-rank test.

(D) Experimental setup for the generation of fumarate-treated macrophages for epigenomic analysis.

CellPress
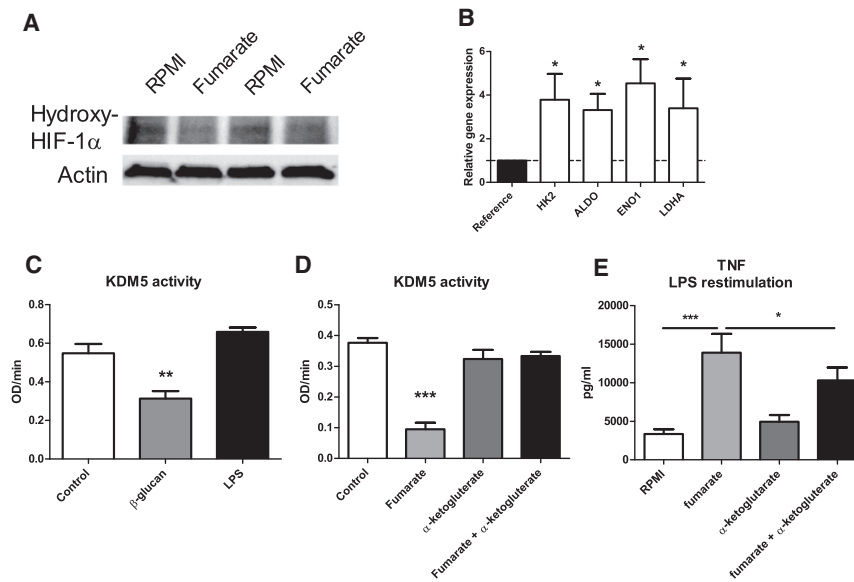
Figure 5. Fumarate Modulates HIF1α Degradation and Epigenetic Modulators

(A) Human monocytes were stimulated for 2 hr with 50 μM fumarate, after which cells were lysed and HIF1α hydroxylation was assessed by western blot. The representative example of five experiments is shown.

(B) Human monocytes were stimulated for 24 hr with 50 μM fumarate, then mRNA was isolated and expression of Hif1α targets was determined. The data are shown as means ± SEM, n = 8, *p < 0.05, and Wilcoxon signed-rank test.

(C) Human monocytes were trained with β-glucan or tolerized with LPS for 24 hr. At day 6, nuclear extracts were isolated and KDM5 activity was determined. The data are shown as means + SEM, n = 6, *p < 0.05, one-way ANOVA, and Dunnett's post test.

(D) Human monocytes were incubated for 24 hr with fumarate or/and α-ketoglutarate after which nuclear extracts were isolated and KDM5 activity was determined. The data are shown as means + SEM, n = 6, *p < 0.05, one-way ANOVA, and Dunnett's post test.

(E) Human monocytes were incubated for 24 hr with fumarate or/and α-ketoglutarate. At day 6, cells were restimulated for 24 hr with LPS and cytokine production was assessed. The data are shown as means + SEM, n = 6, *p < 0.05, one-way ANOVA, and Dunnett's post test.

By using metformin, an activator of AMP kinase and thus inhibitor of mTOR, in healthy volunteers, we demonstrate a role for the mTOR pathway in trained immunity in humans. This observation goes beyond answering a biological question, as metformin is a widely used drug in patients with type 2 diabetes (Singh, 2014). Indeed, its inhibition of trained immunity might have undesired consequences on antimicrobial host defense; on the other hand, it may represent a potential new drug to be employed in certain inflammatory diseases with excessive inflammation (Robey et al., 2015; Singhal et al., 2014; Tan et al., 2015). In contrast to glycolysis, the oxidative branch of PPP does not seem to have a major impact on trained immunity.

Using a systems biology approach, our analysis of intracellular metabolites of trained monocytes identified additional pathways that are involved in trained immunity (Figure 6). The metabolism of several amino acids was enhanced, including glutamine. Metabolism of glutamine into glutamate, α-ketoglutarate, and succinate semialdehyde provides substrates for the TCA cycle such as fumarate and succinate. Interestingly, fumarate itself induces trained immunity as well. Trained immunity induced by fumarate results in increased trimethylation of histones at H3K4, and interestingly also acetylation at H3K27, linking immunometabolic activation with long-term epigenetic changes. Importantly, the epigenetic program induced by fumarate partially reproduces that of β-glucan-induced training, demonstrating its likely involvement in mediating at least part of the effects of β-glucan.

KDMs of the JmjC and JmjD family need α-ketoglutarate as a cofactor for the demethylation process (Lu et al., 2012), whereas

metabolites with a similar molecular structure, such as fumarate, can act as antagonizing factors (Lu et al., 2012; Xiao et al., 2012), thereby inhibiting demethylation. The KDM5 family of demethylases (that is responsible for H3K4 demethylation) has been shown to be inhibited by fumarate (Lu et al., 2012; Xiao et al., 2012). Recently, locally produced fumarate has also been shown to play a role in DNA repair by inhibition of KDM2B histone demethylase activity, which resulted in enhanced H3K36me2 (Jiang et al., 2015). We now show that fumarate inhibits the bioactivity of KDM5s in our model of trained immunity and that α-ketoglutarate can counteract this effect. In addition to fumarate, the concentration of 2-hydroxyglutarate, which has similar antagonizing effects on α-ketoglutarate-dependent demethylases (Yang et al., 2012), is greatly increased in β-glucan-trained macrophages too (Figure S1). Therefore, 2-hydroxyglutarate may serve as another essential factor in modulating histone marks in trained immunity induced by β-glucan. Xiao et al. (2012) have previously shown that fumarate (and potentially 2-hydroxyglutarate) does not only affect histone demethylases, but also affect DNA demethylases. The effect of β-glucan training and metabolic alterations on DNA methylation is therefore an intriguing topic for future research. In addition to the effects of fumarate on epigenetic enzymes, fumarate also inhibits proteasomal degradation of HIF1α, an essential transcription factor in β-glucan-induced trained immunity (Cheng et al., 2014; Koivunen et al., 2007; Serra-Pérez et al., 2010). In this process, α-ketoglutarate is a cofactor for the hydroxylation necessary for HIF1α degradation; fumarate is a natural antagonist of this reaction, thereby stabilizing HIF1α.

(E) Heatmap of H3K4me3 reads (purple) over fumarate-specific peaks. The intensity over the center of the peak ±12 kb is depicted for RPMI-Mf, BG-Mf, and fumarate-Mf, with each row (x axis) corresponding to a peak.

(F) Heatmap of H3K27ac reads (red) over fumarate-specific peaks. The intensity over the center of the peak ±12 kb is depicted for RPMI-Mf, BG-Mf, and fumarate-Mf. The top GO pathways (from DAVID) associated with the nearest genes to dynamic H3K4me3 and H3K27ac are shown, with adjusted p values. See also Figure S5.
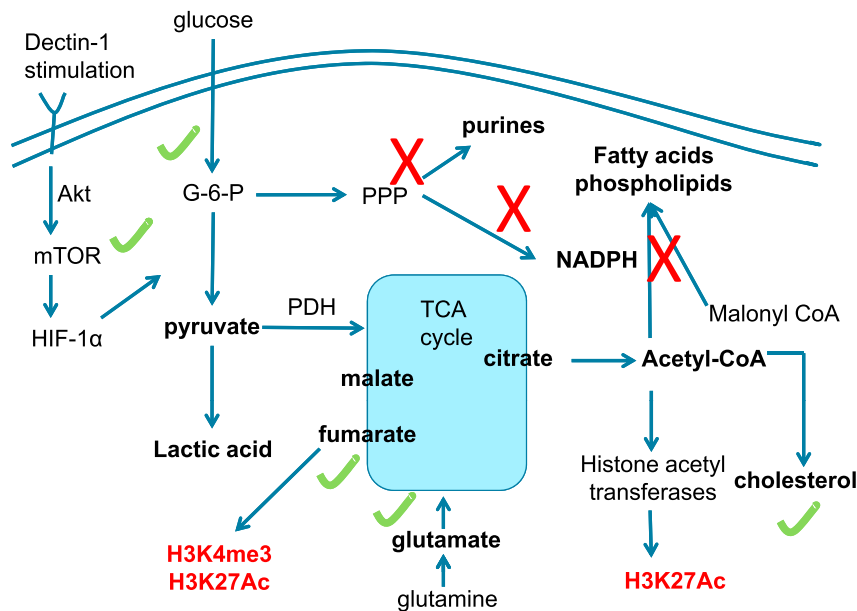
Figure 6. Overview Figure Showing the Metabolic and Epigenetic Pathways through which β-glucan Induces Trained Immunity
Training of monocytes by β-glucan induces complex metabolic pathways: while glycolysis, glutaminolysis, and cholesterol synthesis are important for induction of trained immunity, the PPP and fatty acid synthesis have no direct effect. Fumarate accumulation through glutaminolysis has a central role for induction of histone modifications and induction of trained immunity.

In conclusion, we show that β-glucan-induced trained immunity in monocytes induces profound changes in cellular metabolism. The three most prominent metabolic pathways involved in trained immunity are glycolysis, glutaminolysis, and cholesterol synthesis, which are linked to enrichment in H3K4me3 that is essential for trained immunity by β-glucan. Finally, we provide proof-of-principle of metabolo-epigenomic circuits in innate immune memory by demonstrating an essential role for fumarate in modulating HIF1α degradation, histone methylation, and acetylation. The identification of the metabolic pathways contributing to induction of trained immunity improves understanding of innate immune memory and opens new therapeutic avenues.

EXPERIMENTAL PROCEDURES

Peripheral Blood Mononuclear Cell and Monocyte Isolation
Buffy coats from healthy donors were obtained after written informed consent (Sanquin Blood Bank, Nijmegen, the Netherlands). Peripheral blood mononuclear cell (PBMC) isolation was performed by dilution of blood in pyrogen-free PBS and differential density centrifugation over Ficoll-Paque (GE Healthcare). Cells were washed twice in PBS. Training of adherent monocytes was performed as previously described (Quintin et al., 2012); see also below. Percoll isolation of monocytes was performed as previously described (Repnik et al., 2003). Briefly, 150 − 200 × 10⁶ PBMCs were layered on top of a hyper-osmotic Percoll solution (48.5% Percoll [Sigma-Aldrich], 41.5% sterile H_2O, and 0.16 M filter-sterilized NaCl) and centrifuged for 15 min at 580 × g. The interphase layer was isolated and cells were washed with cold PBS. Cells were resuspended in RPMI culture medium (RPMI medium, Invitrogen) supplemented with 10 μg/mL gentamicin, 10 mM Glutamax, and 10 mM pyruvate, and counted. An extra purification step was added by adhering Percoll-isolated monocytes to polystyrene flat bottom plates (Corning) for 1 hr at 37°C; a washing step with warm PBS was then performed to yield maximal purity.

Monocyte Training and Inhibition Experiments
100 μL cells were added to flat bottom 96-well plates. After washing with warm PBS, monocytes were incubated with culture medium only as a negative control or 5 μg/mL of β-glucan, (β-1,3-(D)-glucan, kindly provided by Professor David Williams), 100 μM mono methyl-fumarate, or dimethyl-2-oxo-glutarate (Sigma) for 24 hr (in 10% pooled human serum). Cells were washed

once with 200 μL warm PBS and incubated for 5 days in culture medium with 10% serum and medium was changed once. Cells were restimulated with 200 μL RPMI, *Escherichia coli* LPS (serotype 055:B5, Sigma-Aldrich, 10 ng/mL), or Pam3Cys (EMC Microcollections, L2000, 10 μg/mL). After 24 hr, supernatants were collected and stored at −20°C (see Figure S1). In some experiments, cells were preincubated (before β-glucan training) for 1 hr with 10 nM rapamycin (Sigma), 50 μM BPTES (Sigma), 2 μg/mL Ceruline (Sigma), 100 μM 6-aminonicotinamide (Sigma), and 20 μM fluvastatin sodium hydrate (Sigma). Concentrations were selected as being the highest non-cytotoxic concentrations.

Cytokine and Lactate Measurements
Cytokine production was determined in supernatants using commercial ELISA kits for TNF-α (R&D Systems) and IL-6 (Sanquin) following the instructions of the manufacturer. Lactate concentration was measured using a Lactate Fluorometric Assay Kit (BioVision).

High-Performance Liquid Chromatography and NMR
Amino acids were quantified by high-performance liquid chromatography (HPLC) in a Gilson UV/vis_155 detector (338 nm) after precolumn derivatization with ortho-phthalaldehyde (OPA with methanol ≥99.9%, potassium borate 1 M pH = 9.5 and 2-mercaptoethanol ≥99.0%) 1:5 (Sigma-Aldrich). Culture supernatants were filtered by Acrodisc 13 mm syringe filters with 0.2 μm supor membrane (Pall). Inorganic mobile phase pH = 7.8 was composed by $Na_2HPO_4.2H_2O_3$ 50 mM: propionic acid 250 mM (1:1) mixture (Merck) with acetonitrile HPLC grade in water (10:2:13). Organic mobile phase was composed by acetonitrile, methanol, and water (3:3:4) (HPLC grade, HiPerSolv Chromanorm, VWR Chemicals). All mobile phases for elution were degasified for 30 min previously to analysis. Amino acids were quantified using the Gilson Uniprot Software, version 5.11 accordingly to standard solutions were prepared in MilliQ water (Millipore).

For NMR spectroscopy, methanol/water extracts and cell culture supernatants were analyzed. The aqueous and chloroform extracts were dried in a SpeedVac Plus system. The aqueous extract was suspended in 600 μL D_2O with 0.262 mM of TSP-d4 as chemical shift indicator and the organic extract in 600 μL CD_3Cl. To 550 μL of cell culture media were added 50 μL D_2O, with a TSP-d4 final concentration of 0.262 mM.

The samples were analyzed at 25°C by ¹H-NMR and by 2D ¹³C-¹H- heteronuclear single quantum coherence (HSQC) spectroscopy in a UltrashiedTM 800 Plus (Bruker) operating at 800.33 MHz, equipped with a TXI-Z H C/N/-D (5 mm) probe. The ¹H-NMR pulse sequence used has a NOESY-presaturation (*noesygppr1d*) with irradiation at the water frequency (ns 124, TD 64K, SW 20 ppm, d1 4 s, d8 0.01 s); while in the ¹³C-¹H-HSQC was used the *hsqcetgpsisp2* pulse sequence (ns 16, TD1 512, TD2 2K, SW2 16 ppm, SW1 165 ppm, d1 1 s). The chemical shifts in aqueous sample were referred to TSP, while the samples in chloroform-d were referred to the solvent signal. Spectra were acquired and processed using TopSpin 3.2 software (Bruker); assignments were made by comparison with chemical shifts found in the literature for metabolic intermediates and Human Metabolome Database (http://www.hmdb.ca). The quantifications of the signals were performed by

integration of the peaks in the ^{1}H-NMR spectra and of the volumes in the ^{13}C-^{1}H-HSQC spectra, using the resonance due to the TSP as reference.

Metabolite Measurements

Cells were cultured as described above. At day 6, cells were detached from the plate with Versene (Life Technologies) and counted. At least one million cells were lysed in 60 μL 0.5% Triton-X in PBS. Metabolite concentrations were determined by commercial assay kits for Acetyl CoA, fumarate, glutamate, malate, NADPH, α-ketoglutarate (all Sigma), following the instructions of the manufacturer.

mRNA Extraction and RT-PCR

Cells were cultured as described above, after 4 hr, 12 hr, and 24 hr for fumarate stimulation or after 6 days after β-glucan training mRNA was extracted by TRIzol (Life Technologies), according to the manufacturer's instruction, and cDNA was synthesized using iScript reverse transcriptase (Invitrogen). Relative mRNA levels were determined using the Applied Biosciences StepOne PLUS and the SYBR Green method (Invitrogen). Values are expressed as fold increases in mRNA levels, relative to those in non-trained cells, with β-2-microglobulin or HPRT as housekeeping genes. Primers are listed in Table S4. RNA-sequencing was performed as described before (Saeed et al., 2014) (GEO: GSE86940 and GSE85246).

Chromatin Immunoprecipitation

10×10^6 monocytes were trained in vitro in 10 cm petri dishes (Greiner) in 10 mL medium volumes. Cells were isolated and trained as described above. After resting for 5 days in culture medium, the cells were detached from the plate with Versene and fixed in methanol-free 1% formaldehyde. Cells were then sonicated and immunoprecipitation was performed using antibodies against H3K4me3 (Diagenode). After ChIP, DNA was processed further for qPCR analysis using SYBR green. Samples were analyzed by a comparative Ct method in which myoglobin was used as a negative control and H2B as a positive control according to the manufacturer's instructions. Primers are listed in Table S4. ChIP sequencing was performed as described before (Saeed et al., 2014).

Metabolome Assessment

Cells were cultured as described above. At 0 hr, 4 hr, 24 hr, and 6 days, cells were harvested and cell pellets were snap frozen and stored at −80°C until metabolite analysis. Measurement of metabolites was performed by liquid chromatography-tandem mass spectrometry (LC-MS). Polar metabolites were extracted in 80% methanol. Metabolic profiles were obtained using three LC-MS methods. Two separate hydrophilic interaction liquid chromatography (HILIC) methods were used to measure polar metabolites in positive and negative ionization mode MS, and one reversed phase method was used to profile lipids in the positive ion mode. Polar metabolites were profiled in the positive ion MS mode using an LC system comprising a 1200 Series Pump (Agilent Technologies) and an HTS PAL Autosampler (Leap Technologies) that was coupled to a 4000 QTRAP mass spectrometer (AB SCIEX) equipped with an electrospray ionization source. Samples were prepared by drying 100 mL of cell extracts under nitrogen and resuspending the residue in 100 mL of 10/67.4/22.4/0.2 v/v/v/v water/acetonitrile/methanol/formic acid containing stable-isotope labeled internal standards (valine-d8, Sigma-Aldrich; and phenylalanine-d8, Cambridge Isotope Laboratories). The samples were centrifuged (10 min, 1,610 × g, 4 μC), and the supernatants were injected directly onto a 150 mm 32.1 mm Atlantis HILIC column (Waters). The column was eluted isocratically with 5% mobile phaseA (10 mM ammonium formate/0.1% formic acid) for 1 min followed by a linear gradient to 40% mobile phase B (acetonitrile/0.1% formic acid) over 10 min. The ion spray voltage was 4.5 kV and the source temperature was 425 μC. All metabolites were measured using several reaction monitoring scans (MRM). MS settings, including declustering potentials and collision energies, for each metabolite were optimized by infusion of reference standards before sample analyses.

MultiQuant software (version 1.2; AB SCIEX) was used to process all raw LC-MS data and integrate chromatographic peaks. The processed data were manually reviewed for quality of integration and compared against known standards to confirm metabolite identities.

Metabolomics Preprocessing
Missing Values
If no peak was detected for a certain metabolite in a particular sample, its concentration was assumed to be below the detection limit. A value of half the minimum value of that metabolite over all samples was used for these metabolites. In doing this, we assume that the minimum value found for a particular metabolite is close to the detection limit.
Data Scaling
The metabolomics data were log2 transformed before most of the analyses were performed (exceptions are mentioned in the next sections). Depending on the type of analysis, different additional scaling steps were performed.

Metformin Proof-of-Principle Trial
The oral metformin study was performed in 12 healthy volunteers, all of whom provided written informed consent. Exclusion criteria consisted of obesity, kidney failure, or metabolic disorders. Volunteers received increasing dosages of metformin for a total of 5 days (500 mg on day 1 and 2,000 mg on day 6). Blood sampling was performed 1 day before start of metformin (day 0), during metformin intake (day 6), on day 9, and on day 20. The study was approved by the local institutional review board (Arnhem-Nijmegen Medical Ethical Committee) and conducted according to the principles of the International Conference on Harmonization-Good Clinical Practice guidelines.

Animal Experiments
C57BL/6J mice were trained by intraperitoneal injection with 1 mg β-glucan as previously described (Quintin et al., 2012). At 1 hr before and 2 hr after intraperitoneal injection of β-glucan or PBS, mice received an intraperitoneal injection of PBS, 200 μg BPTES, or 125 μg atorvastatine. After 7 days, mice were challenged with 10 μg LPS intraperitoneally; after 3 hr, mice were sacrificed and circulating IL-1μ and TNF concentrations were measured by ELISA (R&D Systems) according to the manufacturer's instructions. The study was approved by the ethical animal committee of the University of Colorado, Denver.

KDM5 Activity Assay
Nuclear extracts were prepared according to the method of Schreiber et al. (1990). Cells were cultured as described above, 24 hr for fumarate or α-ketoglutarate stimulation and 5 days after 24 hr stimulation with β-glucan or LPS in 10 cm petri dishes. 1×10^6 cell were resuspended in 400 μl cell lysis buffer (10 mM HEPES; pH 7.5, 10 mM KCl, 0.1 mM EDTA, 1 mM DTT, 0.5% Nonidet-40, and 0.5 mM PMSF along with the protease inhibitor cocktail [Sigma]) and allowed to swell on ice for 20 min with intermittent mixing. Tubes were vortexed and then centrifuged at 12,000 × g at 4°C for 10 min. The pelleted nuclei were washed twice with the cell lysis buffer and resuspended in 25 μL ice-cold nuclear extraction buffer (20 mM HEPES [pH 7.5], 400 mM NaCl, 1 mM EDTA, 1 mM DTT, and 1 mM PMSF with protease inhibitor cocktail) and incubated in ice for 30 min with intermitted sonication. Nuclear extract was collected by centrifugation at 12,000 × g for 15 min at 4°C. The supernatant was used immediately in a fluorometric KDM5/JARID Activity Quantification Assay Kit (Abcam), performed following the instructions of the company.

Analysis Methods
Principal Component Analysis
In the principal component analysis (PCA) of the metabolomics data, the data were first mean-centered. PCA was performed using the function "prcomp" from the "stats" package, part of the "R" language.
Univariate Statistical Testing
For the univariate statistical tests, no further scaling was performed. p values were calculated using a two-sided paired t test, using the function "t.test," part of the "R" language. p values were corrected using the Benjamini-Hochberg false discovery rate procedure (as implemented in R). Pathway enrichment analysis: Pathway enrichment analysis was performed using two different methods. The first was "Pathway-tools" (Chen et al., 2014), the stand-alone version of the tool integrated into the Biocyc online resource (Caspi et al., 2014). This tool allows additional visualization of the data on a metabolic pathway map (both metabolomic and transcriptomic), but this tool does not allow the definition of a background metabolic set (all metabolites measured by the used platform). Pathway-tools require the definition of a set of significantly differentially expressed metabolites/genes. Metabolites and genes

were defined as significantly changed between two conditions if they had a FDR <0.1. The second method used to perform pathway-enrichment analysis is "MetaboAnalyst" (Xia et al., 2015), which does allow the definition of such a background set. MetaboAnalyst additionally has the advantage of performing a quantitative enrichment analysis instead of using a hard threshold, however, it does not allow the type of visualization that is provided by Pathway-tools. This complementary set of options was the reason for using both tools. A quantitative enrichment analysis was performed using the peak intensities as an input (before log2 transform). The settings were as follows: missing values were imputed as explained in Metabolomics Preprocessing and no data filtering or scaling was applied. The pathway-associated metabolite sets were used to check for enrichment (before and after log transformation), using all metabolites measured with mass spectrometry as a custom reference set. Pathways of less than four compounds were filtered from our analysis. p values for enriched pathways in both methods were corrected using the Benjamini-Hochberg false discovery rate procedure.

Data Visualization
The first explorative visualization was performed using Pathway-tools, which allows visualization of both transcriptomic and metabolomic data. Based on the pathways that were significantly differentially expressed in either the metabolomic or transcriptomic data, the interesting parts of the map were explored. Next, using the tool "Escher" (King et al., 2015), a pathway map was created, containing just the parts found to be of interest. A schematic overview of the pathways is depicted in Figure 1C (the complete map as created by Escher is depicted in Figure S1).

Statistics
Ex vivo and in vitro monocyte experiments were analyzed using a Wilcoxon signed-rank test or one-way ANOVA, where applicable. A p value below 0.05 was considered statistically significant. These data were analyzed using GraphPad Prism 5.0. *p < 0.05 and **p < 0.01. Data are shown as means ± SEM.

ACCESSION NUMBERS

The accession numbers for the RNA sequencing time course of control, β-glucan-trained, and LPS-immunotolerant monocytes and RNA sequencing and ChIP sequencing data of control and fumarate- and β-glucan-trained monocytes at day 6 reported in this paper are GEO: GSE85246 and GSE86940.

SUPPLEMENTAL INFORMATION

Supplemental Information includes Supplemental Experimental Procedures, six figures, and four tables and can be found with this article online at http://dx.doi.org/10.1016/j.cmet.2016.10.008.

AUTHOR CONTRIBUTIONS

Conceptualization: R.J.W.A., B.N., R.t.H., S.-C.C., F.L.v.d.V., J.W.M.v.d.M., C.A.D., L.A.B.J., and M.G.N.; Formal Analysis and Investigation: R.J.W.A., B.N., R.t.H., S.B., E.L., F.R., R.S., S.-C.C., S.-Y.W., E.H., L.G.G., I.M., C. Cunha, A.v.L., and C. Clish; Resources: D.L.W. and L.A.B.J.; Writing - Original Draft: R.J.W.A., B.N., and M.G.N.; Writing - Review & Editing: A.C., F.L.v.d.V., L.A.O.N., N.P.R., R.v.C., R.A.N., H.G.S., R.J.X., and M.G.N.; and Supervision: A.C., C.L., N.P.R., R.v.C., C. Clish, R.A.N., L.A.B.J., H.G.S., and M.G.N.

ACKNOWLEDGMENTS

REFERENCES

Caspi, R., Altman, T., Billington, R., Dreher, K., Foerster, H., Fulcher, C.A., Holland, T.A., Keseler, I.M., Kothari, A., Kubo, A., et al. (2014). The MetaCyc database of metabolic pathways and enzymes and the BioCyc collection of Pathway/Genome Databases. Nucleic Acids Res. 42, D459–D471.

Chen, Q., Giedt, M., Tang, L., and Harrison, D.A. (2014). Tools and methods for studying the Drosophila JAK/STAT pathway. Methods 68, 160–172.

Cheng, S.C., Quintin, J., Cramer, R.A., Shepardson, K.M., Saeed, S., Kumar, V., Giamarellos-Bourboulis, E.J., Martens, J.H., Rao, N.A., Aghajanirefah, A., et al. (2014). mTOR- and HIF-1α-mediated aerobic glycolysis as metabolic basis for trained immunity. Science 345, 1250684.

Cheng, S.C., Scicluna, B.P., Arts, R.J., Gresnigt, M.S., Lachmandas, E., Giamarellos-Bourboulis, E.J., Kox, M., Manjeri, G.R., Wagenaars, J.A., Cremer, O.L., et al. (2016). Broad defects in the energy metabolism of leukocytes underlie immunoparalysis in sepsis. Nat. Immunol. 17, 406–413.

Donohoe, D.R., and Bultman, S.J. (2012). Metaboloepigenetics: interrelationships between energy metabolism and epigenetic control of gene expression. J. Cell. Physiol. 227, 3169–3177.

Fu, Z.Q., and Dong, X. (2013). Systemic acquired resistance: turning local infection into global defense. Annu. Rev. Plant Biol. 64, 839–863.

Hirschey, M.D., DeBerardinis, R.J., Diehl, A.M., Drew, J.E., Frezza, C., Green, M.F., Jones, L.W., Ko, Y.H., Le, A., Lea, M.A., et al.; Target Validation Team (2015). Dysregulated metabolism contributes to oncogenesis. Semin. Cancer Biol. 35 (Suppl), S129–S150.

Jiang, Y., Qian, X., Shen, J., Wang, Y., Li, X., Liu, R., Xia, Y., Chen, Q., Peng, G., Lin, S.Y., and Lu, Z. (2015). Local generation of fumarate promotes DNA repair through inhibition of histone H3 demethylation. Nat. Cell Biol. 17, 1158–1168.

Ke, Q., and Costa, M. (2006). Hypoxia-inducible factor-1 (HIF-1). Mol. Pharmacol. 70, 1469–1480.

Keating, S.T., and El-Osta, A. (2015). Epigenetics and metabolism. Circ. Res. 116, 715–736.

King, Z.A., Dräger, A., Ebrahim, A., Sonnenschein, N., Lewis, N.E., and Palsson, B.O. (2015). Escher: A web application for building, sharing, and embedding data-rich visualizations of biological pathways. PLoS Comput. Biol. 11, e1004321.

Kleinnijenhuis, J., Quintin, J., Preijers, F., Joosten, L.A., Ifrim, D.C., Saeed, S., Jacobs, C., van Loenhout, J., de Jong, D., Stunnenberg, H.G., et al. (2012). Bacille Calmette-Guerin induces NOD2-dependent nonspecific protection from reinfection via epigenetic reprogramming of monocytes. Proc. Natl. Acad. Sci. USA 109, 17537–17542.

Koivunen, P., Hirsilä, M., Remes, A.M., Hassinen, I.E., Kivirikko, K.I., and Myllyharju, J. (2007). Inhibition of hypoxia-inducible factor (HIF) hydroxylases by citric acid cycle intermediates: possible links between cell metabolism and stabilization of HIF. J. Biol. Chem. 282, 4524–4532.

Kurtz, J. (2005). Specific memory within innate immune systems. Trends Immunol. 26, 186–192.

Li, P., Yin, Y.L., Li, D., Kim, S.W., and Wu, G. (2007). Amino acids and immune function. Br. J. Nutr. 98, 237–252.

Lu, C., Ward, P.S., Kapoor, G.S., Rohle, D., Turcan, S., Abdel-Wahab, O., Edwards, C.R., Khanin, R., Figueroa, M.E., Melnick, A., et al. (2012). IDH mutation impairs histone demethylation and results in a block to cell differentiation. Nature 483, 474–478.

Mills, E.L., and O'Neill, L.A. (2015). Reprogramming mitochondrial metabolism in macrophages as an anti-inflammatory signal. Eur. J. Immunol 46, 13–21.

Muthamilarasan, M., and Prasad, M. (2013). Plant innate immunity: an updated insight into defense mechanism. J. Biosci. 38, 433–449.

Netea, M.G., Quintin, J., and van der Meer, J.W. (2011). Trained immunity: a memory for innate host defense. Cell Host Microbe 9, 355–361.

Netea, M.G., Joosten, L.A., Latz, E., Mills, K.H., Natoli, G., Stunnenberg, H.G., O'Neill, L.A., and Xavier, R.J. (2016). Trained immunity: A program of innate immune memory in health and disease. Science 352, aaf1098.

O'Sullivan, T.E., Sun, J.C., and Lanier, L.L. (2015). Natural killer cell memory. Immunity 43, 634–645.

Pearce, E.L., Poffenberger, M.C., Chang, C.H., and Jones, R.G. (2013). Fueling immunity: insights into metabolism and lymphocyte function. Science 342, 1242454.

Quintin, J., Saeed, S., Martens, J.H., Giamarellos-Bourboulis, E.J., Ifrim, D.C., Logie, C., Jacobs, L., Jansen, T., Kullberg, B.J., Wijmenga, C., et al. (2012). Candida albicans infection affords protection against reinfection via functional reprogramming of monocytes. Cell Host Microbe 12, 223–232.

Repnik, U., Knezevic, M., and Jeras, M. (2003). Simple and cost-effective isolation of monocytes from buffy coats. J. Immunol. Methods 278, 283–292.

Robey, R.B., Weisz, J., Kuemmerle, N.B., Salzberg, A.C., Berg, A., Brown, D.G., Kubik, L., Palorini, R., Al-Mulla, F., Al-Temaimi, R., et al. (2015). Metabolic reprogramming and dysregulated metabolism: cause, consequence and/or enabler of environmental carcinogenesis? Carcinogenesis 36 (Suppl 1), S203–S231.

Roth, E. (2008). Nonnutritive effects of glutamine. J. Nutr. 138, 2025S–2031S.

Saeed, S., Quintin, J., Kerstens, H.H., Rao, N.A., Aghajanirefah, A., Matarese, F., Cheng, S.C., Ratter, J., Berentsen, K., van der Ent, M.A., et al. (2014). Epigenetic programming of monocyte-to-macrophage differentiation and trained innate immunity. Science 345, 1251086.

Schreiber, E., Harshman, K., Kemler, I., Malipiero, U., Schaffner, W., and Fontana, A. (1990). Astrocytes and glioblastoma cells express novel octamer-DNA binding proteins distinct from the ubiquitous Oct-1 and B cell type Oct-2 proteins. Nucleic Acids Res. 18, 5495–5503.

Secombe, J., and Eisenman, R.N. (2007). The function and regulation of the JARID1 family of histone H3 lysine 4 demethylases: the Myc connection. Cell Cycle 6, 1324–1328.

Serra-Pérez, A., Planas, A.M., Núñez-O'Mara, A., Berra, E., García-Villoria, J., Ribes, A., and Santalucía, T. (2010). Extended ischemia prevents HIF1alpha degradation at reoxygenation by impairing prolyl-hydroxylation: role of Krebs cycle metabolites. J. Biol. Chem. 285, 18217–18224.

Shah, J., Chaturvedi, R., Chowdhury, Z., Venables, B., and Petros, R.A. (2014). Signaling by small metabolites in systemic acquired resistance. Plant J. 79, 645–658.

Sikalidis, A.K. (2015). Amino acids and immune response: a role for cysteine, glutamine, phenylalanine, tryptophan and arginine in T-cell function and cancer? Pathol. Oncol. Res. 21, 9–17.

Singh, S. (2014). Type 2 diabetes pharmacoepidemiology update 2014: safety versus efficacy. Curr. Diab. Rep. 14, 563.

Singhal, A., Jie, L., Kumar, P., Hong, G.S., Leow, M.K., Paleja, B., Tsenova, L., Kurepina, N., Chen, J., Zolezzi, F., et al. (2014). Metformin as adjunct antituberculosis therapy. Sci. Transl. Med. 6, 263ra159.

Sun, J.C., Beilke, J.N., and Lanier, L.L. (2009). Adaptive immune features of natural killer cells. Nature 457, 557–561.

Tan, Z., Xie, N., Cui, H., Moellering, D.R., Abraham, E., Thannickal, V.J., and Liu, G. (2015). Pyruvate dehydrogenase kinase 1 participates in macrophage polarization via regulating glucose metabolism. J. Immunol. 194, 6082–6089.

Tannahill, G.M., Curtis, A.M., Adamik, J., Palsson-McDermott, E.M., McGettrick, A.F., Goel, G., Frezza, C., Bernard, N.J., Kelly, B., Foley, N.H., et al. (2013). Succinate is an inflammatory signal that induces IL-1β through HIF-1α. Nature 496, 238–242.

Van den Bossche, J., Baardman, J., and de Winther, M.P. (2015). Metabolic characterization of polarized M1 and M2 bone marrow-derived macrophages using real-time extracellular flux analysis. J. Vis. Exp. http://dx.doi.org/10.3791/53424.

Xia, J., Sinelnikov, I.V., Han, B., and Wishart, D.S. (2015). MetaboAnalyst 3.0–making metabolomics more meaningful. Nucleic Acids Res. 43, W251–W257.

Xiao, M., Yang, H., Xu, W., Ma, S., Lin, H., Zhu, H., Liu, L., Liu, Y., Yang, C., Xu, Y., et al. (2012). Inhibition of α-KG-dependent histone and DNA demethylases by fumarate and succinate that are accumulated in mutations of FH and SDH tumor suppressors. Genes Dev. 26, 1326–1338.

Yang, H., Ye, D., Guan, K.L., and Xiong, Y. (2012). IDH1 and IDH2 mutations in tumorigenesis: mechanistic insights and clinical perspectives. Clin. Cancer Res. 18, 5562–5571.

Supplemental Information

Glutaminolysis and Fumarate Accumulation

Integrate Immunometabolic and Epigenetic

Programs in Trained Immunity

Rob J.W. Arts, Boris Novakovic, Rob ter Horst, Agostinho Carvalho, Siroon Bekkering, Ekta Lachmandas, Fernando Rodrigues, Ricardo Silvestre, Shih-Chin Cheng, Shuang-Yin Wang, Ehsan Habibi, Luís G. Gonçalves, Inês Mesquita, Cristina Cunha, Arjan van Laarhoven, Frank L. van de Veerdonk, David L. Williams, Jos W.M. van der Meer, Colin Logie, Luke A. O'Neill, Charles A. Dinarello, Niels P. Riksen, Reinout van Crevel, Clary Clish, Richard A. Notebaart, Leo A.B. Joosten, Hendrik G. Stunnenberg, Ramnik J. Xavier, and Mihai G. Netea
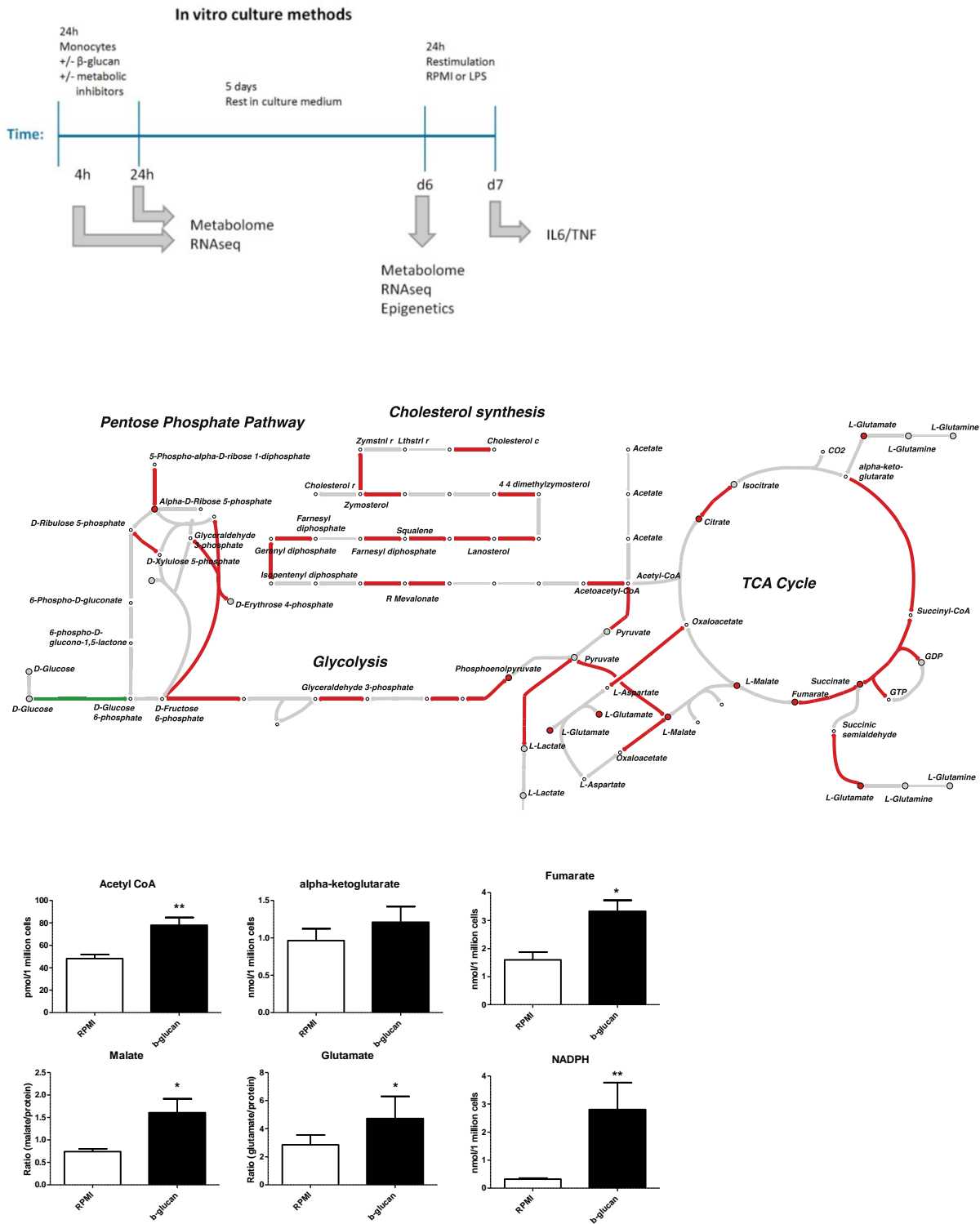
Figure S1. Related to Figure 1-5. Experimental setup. Monocytes were isolated from buffy coats and plated to flat-bottom plates. Cells were 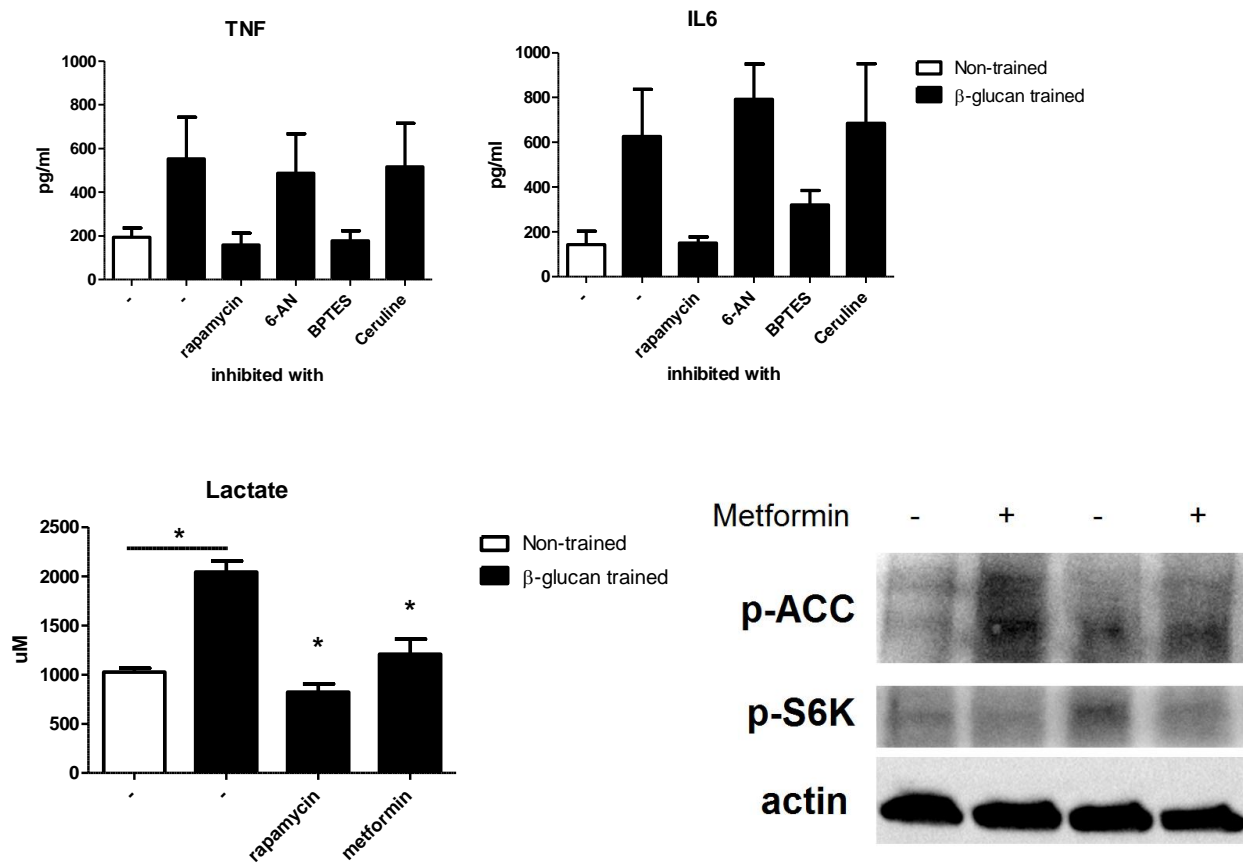left to adhere for 1 h and were washed once with warm PBS to reach maximum purity. Then, depending on the experiment inhibitors and/or β-glucan were added. After 24h incubation, cells were washed once with warm PBS and were left to rest in culture medium for five days (with one medium change half way). At day six, cells were restimulated for 24h with RPMI of 10ng/ml LPS. The experiment was terminated at several time points as depicted. Metabolome and RNA-seq samples were taken directly after 4 h, 24 h and 6 days. Epigenetic analysis was always performed on day six, prior to restimulation. And cytokines were always determined after the whole protocol was finished.

At day 6, cells were lysed and intracellular concentrations of metabolites were determined. Metabolites are shown as circles; reactions are shown as arrows. Significantly upregulated (red), downregulated (green), and unchanged (gray) reactions/metabolites are shown. Metabolites that were not measured are depicted as small-unfilled circles. Figure was created using the tool "Escher."

Highlight of the ^{1}H-^{13}C HSQC-NMR spectra of monocytes (methanol extracts) cultured with [2-^{13}C]-glucose that were unstimulated (black) or stimulated with β-glucan (red). The ^{13}C from the glucose was incorporated in the position 2 of lactate (Lac-2) in both conditions and in the rybosyl moiety of nucleotides (Rib-1, Rib-3 and Rib-4) when the cells were stimulated with β-glucan.

Highlight of the ^{1}H-^{13}C HSQC-NMR spectra of monocytes(methanol extracts) cultured with [U-^{13}C]-glutamine that were unstimulated (black) or stimulated with β-glucan (red). The ^{13}C from glutamine was presented in glutamine (Gln) in both conditions and in glutamate (Glu) and glutamyl moiety of glutathione (GSH) when the cells were stimulated with β-glucan.

Figure: Highlight of the ^{1}H-^{13}C HSQC-NMR spectra of the culture media after growth cultured with [2-13C]-glucose that were unstimulated (black) or stimulated with β-glucan (red). The ^{13}C from the glucose was incorporated in the position 2 of lactate (Lac-2) in both conditions.

Highlight of the ^{1}H-^{13}C HSQC-NMR spectra of culture media after growth with [U-^{13}C]-glutamine that were unstimulated (black) or stimulated with β-glucan (red). The ^{13}C from glutamine was presented in glutamine (Gln), glutamate (Glu) and pyroglutamate (Glp) in both conditions. It is also observed lactate (Lac) and glucose (glc) but is not labelled.

Figure S2. Related to Figure 2A and 3A. ^{1}H-^{13}C HSQC-NMR spectra. The destination of ^{13}C labeled glucose (left) or glutamine (right) was determined in β-glucan vs non-trained monocytes by NMR both in cells (upper) and culture medium (lower panels).

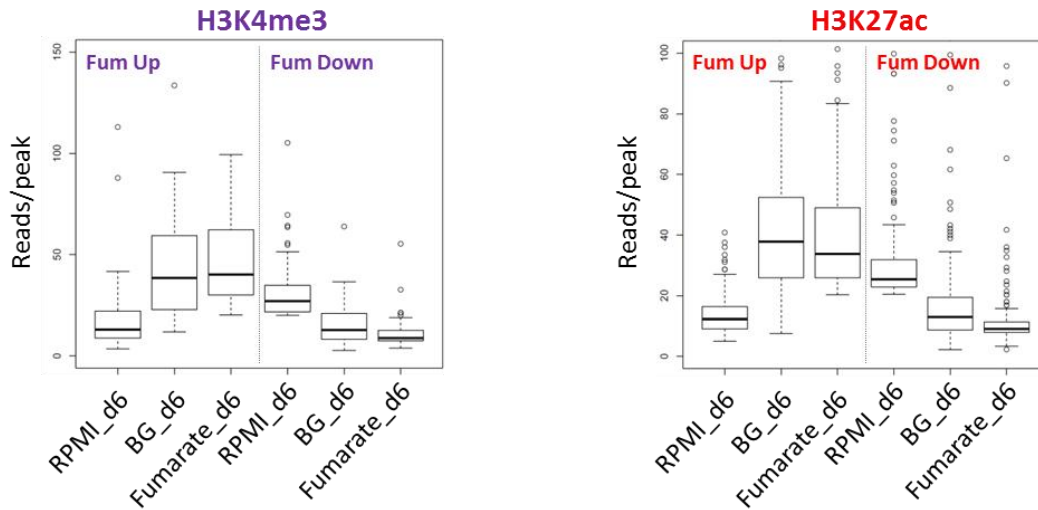**Figure S3. Related to Figure 2&3.** Human monocytes were incubated for 24h with β-glucan in the presence of absence of metabolic inhibitors in 10cm petri dishes. After 24h cells were washed and 10% serum in RPMI was added, on day 3 medium was changed. On day 6 cells were washed once with warm PBS. The adherent macrophages were deattached and 50.000 cells were reseeded in 96-well flat-bottom plates and stimulated with RPMI or 10ng/ml LPS for 24h and cytokine and lactate production were assessed. RPMI restimulated cells did not produce TNF or IL6. **Metformin activates AMPK and inhibits mTOR.** Human monocytes were incubated for 2h with 3mM of metformin, then cells were lysed and phosphorylation of ACC (downstream target of AMPK) and S6K (downstream target of mTOR) were assessed by Western Blotting.
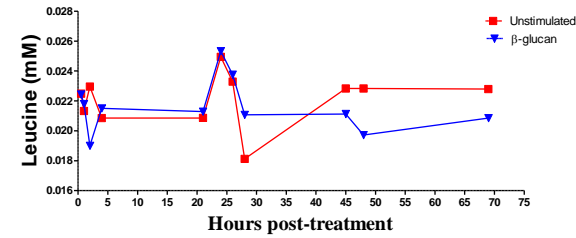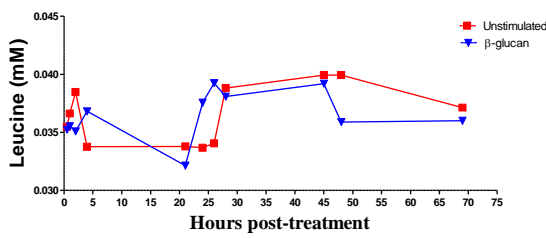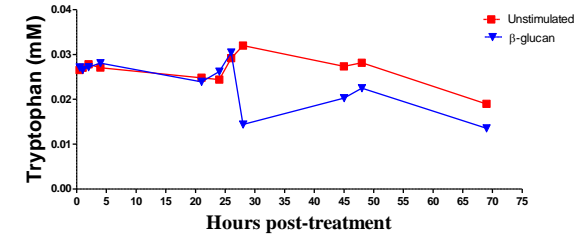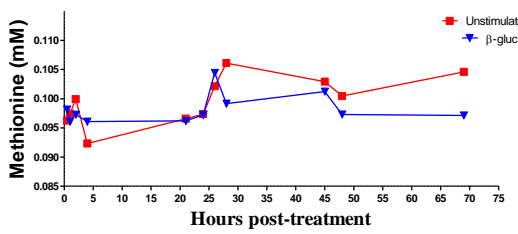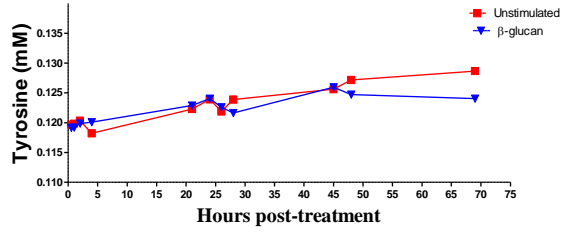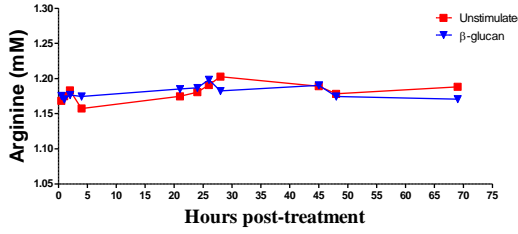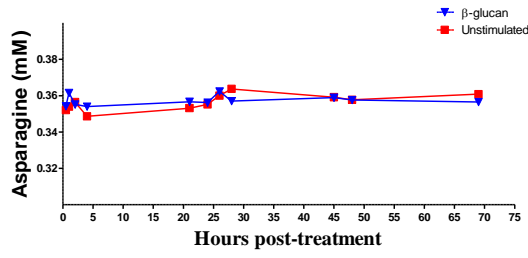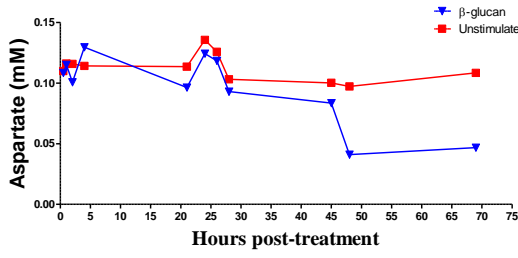
Figure S4. Related to Figure 3. Amino acid consumption during β-glucan-induced trained immunity. Monocytes were trained with β-glucan for 24 h. Post-treatment amino acid concentrations in the culture medium were determined at indicated time points. Culture medium was changed once after 24 h.

A

H3K4me3

Fum Up   Fum Down

Reads/peak

RPMI_d6 BG_d6 Fumarate_d6 RPMI_d6 BG_d6 Fumarate_d6

H3K27ac

Fum Up   Fum Down

Reads/peak

RPMI_d6 BG_d6 Fumarate_d6 RPMI_d6 BG_d6 Fumarate_d6

B

Top GO for H3K4me3 Fumarate Up associated genes

DAVID GO biological process and KEGG pathways	P.adj
positive regulation of immune system process	5.70E-03
regulation of T-helper 1 type immune response	1.10E-02
positive regulation of leukocyte activation	1.20E-02
positive regulation of cell activation	1.30E-02
immune response	2.00E-02
regulation of leukocyte activation	2.70E-02
regulation of cell activation	3.00E-02
T cell proliferation	4.10E-02
Cytokine-cytokine receptor interaction	6.30E-01

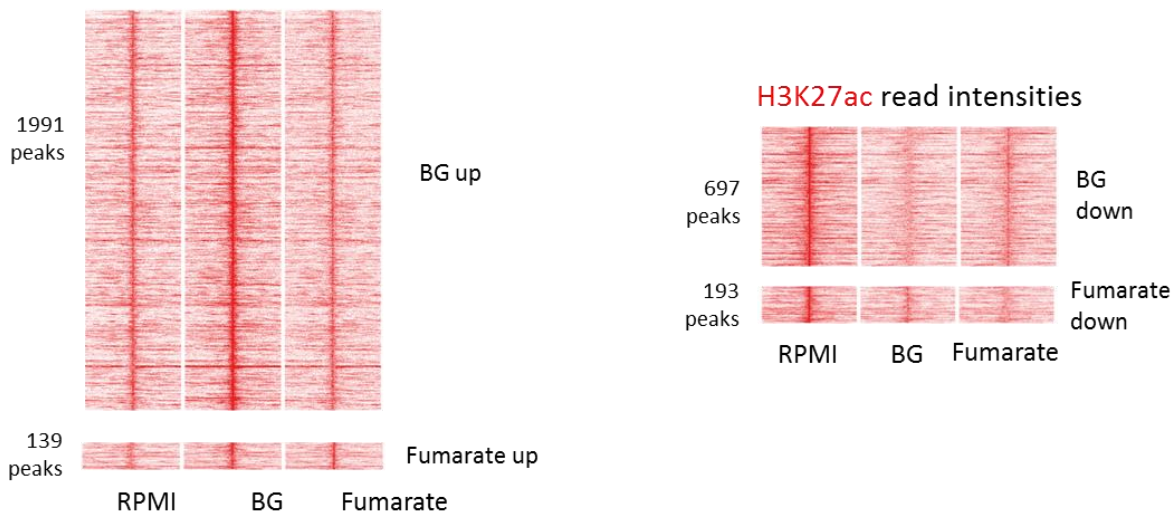| Genes In top pathways |
|---|
| ADORA2B |
| IL4R |
| SLC11A1 |
| TNFSF14 |
| CCL22 |

Fumarate down
No significant enrichment in DAVID or GREAT

Top GO for H3K27ac Fumarate Up associated genes

GREAT pathway	P.adj
leukocyte migration	1.55E-02
regulation of intracellular protein kinase cascade	1.47E-02
cellular response to abiotic stimulus	4.42E-02

Fumarate down

GREAT and DAVID pathway	P.adj
regulation of immune system process	1.62E-02
regulation of cell activation	4.56E-02
estrous cycle phase	3.13E-02
regulation of specific transcription from RNA polymerase II promoter	7.80E-02

Genes In top pathways
ANGPT4
CD48
CXCL3
CXCR4
EPS8
FN1
PRKCA
SLC7A11
SPP1
SRC
ACTN1

C

H3K27ac read intensities for BG induced and Fumarate induced changes

1991 peaks — BG up

139 peaks — Fumarate up

RPMI   BG   Fumarate

H3K27ac read intensities

697 peaks — BG down

193 peaks — Fumarate down

RPMI   BG   Fumarate

Figure S5. Related to Figure 4E,F. Epigenetic analysis of fumarate-induced trained macrophages. β-glucan- and fumarate-induced epigenetic changes. (A) Boxplots of H3K4me3 and H3K27ac reads/peak for fumarate "up" and fumarate "down" peaks. (B) Dynamic H3K4me3 and H3K27ac peaks (genomic regions with signal) were assigned to the nearest protein-coding gene using GREAT (http://bejerano.stanford.edu/great/public/html/). The top pathways from GREAT or DAVID gene ontology tools are shown as a table. Selected genes in the top pathways are also shown. (C) Heat map showing H3K27ac signal intensity at regions that are modulated by β-glucan ("BG up" and "BG down") or fumarate ("Fumarate up" and "Fumarate down"). Each row of the heat map is a peak, and the y axis shows distance from the center of the peak (+/- 12kb). The height of the heat map corresponds to the number of peaks.
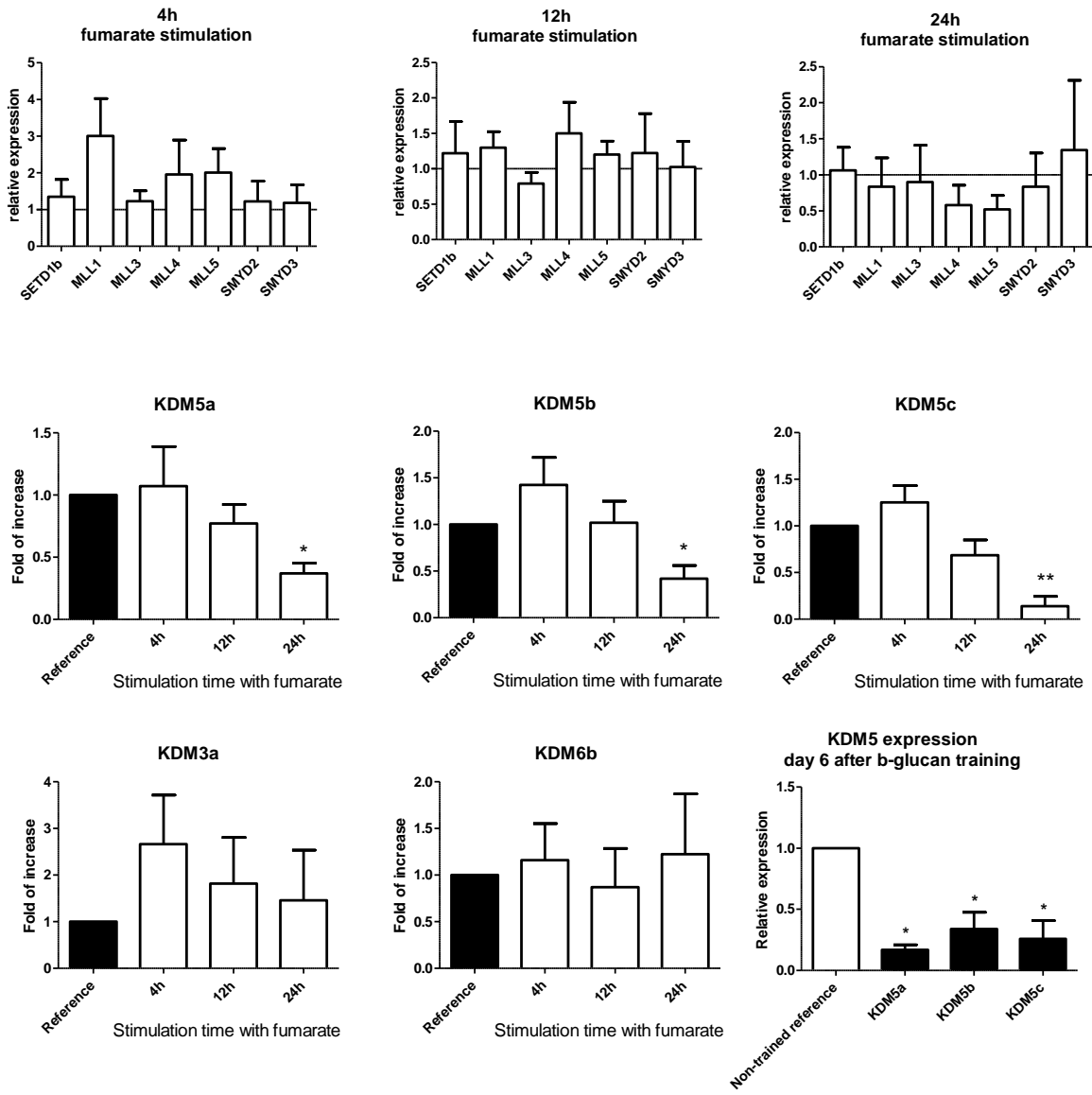
Figure S6. Related to Figure 5. Modulatation of epigenetic enzymes by fumarate. Human monocytes were stimulated for 4 h, 12 h, and 24 h with 50 μM fumarate, after which mRNA was isolated and expression of histone methyltransferases or demethylases was determined. Or human monocytes were trained with β-glucan. After 24h cells were washed and after 5 days of rest KDM5 expression was determined.

Supplemental Tables

Table S1, related to Figure 1 and Figure S1. Pathway enrichment based on the metabolomics data constructed with the MetaboAnalyst tool (with all measured metabolites as a background). Raw data intensities were used for analysis. Details of the procedure are described in Methods.

Table S2, related to Figure 1 and Figure S1. Pathway enrichment of upregulated metabolites based on the metabolomics data constructed with the Pathway-tools tool. Metabolites were considered significant if they have a FDR (Benjamini-Hochberg) of < 0.1. Details of the procedure are described in Methods.

Table S3, related to Figure 1 and Figure S1. Pathway enrichment based on the transcriptomics data constructed with the Pathway-tools tool. Genes were considered significant if they have a FDR (Benjamini-Hochberg) of < 0.1. Details of the procedure are described in Methods.

Table S4, related to Figure 6. Primers used for qPCR.

Epigenetic promoter primers		
Gene	Forward (5'-->3')	Reverse (5'-->3')
Myoglobulin	AGCATGGTGCCACTGTGCT	GGCTTAATCTCTGCCTCATGAT
H2B	TGTACTTGGTGACGGCCTTA	CATTACAACAAGCGCTCGAC
TNF	GTGCTTGTTCCTCAGCCTCT	ATCACTCCAAAGTGCAGCAG
IL6	AGGGAGAGCCAGAACACAGA	GAGTTTCCTCTGACTCCATCG
qPCR primers		
Gene	Forward (5'-->3')	Reverse (5'-->3')
B2M	ATGAGTATGCCTGCCGTGTG	CCAAATGCGGCATCTTCAAAC
HPRT	CCTGGCGTCGTGATTAGTGAT	AGACGTTCAGTCCTGTCCATAA
Hexokinase2	TTGACCAGGAGATTGACATGGG	CAACCGCATCAGGACCTCA
ALDOA	CAGGGACAAATGGCGAGACTA	GGGGTGTGTTCCCCAATCTT
ENO1	TGGTGTCTATCGAAGATCCCTT	CCTTGGCGATCCTCTTTGG
LDHA	ATGGCAACTCTAAAGGATCAGC	CCAACCCCAACAACTGTAATCT
KDM5a	AGCCGAGTTGGGAGGAGTT	TGGACTCTTGGAGTGAAACGA
KDM5b	CCATAGCCGAGCAGACTGG	GGATACGTGGCGTAAAATGAAGT
KDM5c	GGGTCCGACGATTCCTACC	ATGCCCGATTTCTCTGCGATG
KDM5d	CAAGACCCGCTTGGCTACATT	TTGGACGCGAGGAGTAAATCT
KDM3a	GTGCTCACGCTCGGAGAAA	GTGGGAAACAGCTCGAATGGT
KDM6b	CACCCCAGCAAACCATATTATGC	CACACAGCCATGCAGGGATT